A new look at the architecture and dynamics of the *Hydra* nerve net

Athina Keramidioti [a,+], Sandra Schneid [a,+], Christina Busse [a,+], Christoph Cramer von Laue [b], Bianca Bertulat [b], Willi Salvenmoser [c], Martin Heß [a], Olga Alexandrova [a], Kristine M. Glauber [d], Robert E. Steele [d], Bert Hobmayer [c] *, Thomas Holstein [b] *, Charles N. David [a] *

(a) Department of Biology, Ludwig-Maximilians-University Munich, 82152 Martinsried, Germany
(b) Centre for Organismal Studies (COS) Heidelberg, Heidelberg University, 69120 Heidelberg, Germany
(c) Department of Zoology and Center for Molecular Biosciences Innsbruck (CMBI), University of Innsbruck, 6020 Innsbruck, Austria
(d) Department of Biological Chemistry, University of California, Irvine, CA 92617, USA

(*) corresponding authors
(+) These authors contributed equally to this paper

email address for correspondence:

Charles N. David	david@bio.lmu.de
Athina Keramidioti	a.keramidiotou@gmail.com
Sandra Schneid	sandra_schneid@hotmail.de
Christina Busse	christina.busse@gmx.com
Olga Alexandrova	oarchilovna@googlemail.com
Martin Heß	hess@zi.biologie.uni-muenchen.de
Thomas W. Holstein	thomas.holstein@cos.uni-heidelberg.de
Christoph Cramer von Laue	chris.laue@gmx.de
Bianca Bertulat	bertulat@em.uni-frankfurt.de
Bert Hobmayer	bert.hobmayer@uibk.ac.at
Willi Salvenmoser	willi.salvenmoser@aon.at
Robert E Steele	resteele@uci.edu
Kristine M. Glauber	kristine.glauber@duke.edu

Abstract

The *Hydra* nervous system is the paradigm of a "simple nerve net". Nerve cells in *Hydra*, as in many cnidarian polyps, are organized in a nerve net extending throughout the body column. This nerve net is required for control of spontaneous behavior: elimination of nerve cells leads to polyps that do not move and are incapable of capturing and ingesting prey (Campbell, 1976). We have re-examined the structure of the *Hydra* nerve net by immunostaining fixed polyps with a novel antibody that stains all nerve cells in *Hydra*. Confocal imaging shows that there are two distinct nerve nets, one in the ectoderm and one in the endoderm, with the unexpected absence of nerve cells in the endoderm of the tentacles. The nerve nets in the ectoderm and endoderm do not contact each other. High-resolution TEM and serial block face SEM show that the nerve nets consist of bundles of parallel overlapping neurites. Results from transgenic lines show that neurite bundles include different neural circuits and hence that neurites in bundles require circuit-specific recognition. Nerve cell-specific innexins indicate that gap junctions can provide this specificity. The occurrence of bundles of neurites supports a model for continuous growth and differentiation of the nerve net by lateral addition of new nerve cells to the existing net. This model was confirmed by tracking newly differentiated nerve cells.

Introduction

Nerve cells arose early in the evolution of multicellular animals to sense the environment and control the activity of downstream effector cells (Anderson, 1990; Mackie, 1990). In non-bilaterians (cnidarians and ctenophores) nerve cells are organized in nerve nets, which are often associated with muscle processes and coordinate the behaviors that involve ectodermal and endodermal tissues (Mackie, 1990). In bilaterian metazoans, the number of nerve cells is commonly much higher than in cnidarians and ctenophores and – importantly – nerves are organized into a centralized nervous system with large ganglia (Arendt et al., 2016). The relatively simple organization of nervous tissue in non-bilaterians offers the possibility of achieving a comprehensive understanding of the relationship between the architecture and activity of the nervous system and animal behavior (Bosch et al., 2017; Galliot et al., 2009; Watanabe et al., 2009).

With a nervous system consisting of only 500-2000 nerve cells, depending on animal size (Bode et al., 1973), the freshwater cnidarian polyp *Hydra* is a particularly useful model organism for such investigations. Furthermore, there are only two types of nerve cells in *Hydra* based on morphology: ganglion cells and sensory cells, and there are no surrounding support cells, such as glial cells in bilaterians (David, 1973; Epp and Tardent, 1978; Westfall, 1973; Westfall and Epp, 1985). Ganglion cells are bipolar or multipolar, but there is no evidence for a distinction between axons and dendrites. Sensory nerve cells, by comparison, are polarized, with a short neurite and sensory cilium at one pole and a longer neurite at the opposite pole. Sensory cells in the ectoderm extend a cilium to the surface of the epithelium to sense the external environment. Sensory cells in the endoderm extend a cilium into the gastric cavity. Recent scRNAseq results have refined these morphological classes to include 3 sensory

and 5 ganglion nerve cell populations based on distinct transcriptomes (Cazet et al., 2023; Siebert et al., 2019).

Nerve cells in *Hydra* are organized in a nerve net, as first described in classic studies (Schneider, 1890; Hadži, 1909), in which the nerves were visualized by methylene blue staining and tissue maceration. Although higher concentrations of nerve cells were found in the head and the foot, there was no evidence for ganglia or a "brain". A more detailed description of the organization and formation of distinct subpopulations of nerve cells in the various body parts of *Hydra* polyps was achieved by using monoclonal antibodies that recognized unknown antigens and antibodies that recognized neuropeptides (Dunne et al., 1985; Grimmelikhuijzen, 1983; Grimmelikhuijzen et al., 1996; Hobmayer et al., 1990a; Hobmayer et al., 1990b; Technau and Holstein, 1996; Yaross et al., 1986). More recently, the use of in situ hybridization to detect the expression of neuropeptide genes and transgenic reporter lines using the promoters from neuropeptide genes have provided more understanding of the regionalization of the peptidergic part of *Hydra*'s nervous system (Hansen et al., 2000; Grimmelikhuijzen et al., 1996; Koizumi et al., 2004; Noro et al., 2019). However, all of these results lacked the resolution to describe the entire nerve net in detail and there is presently no clear understanding of the overall organization of cells in the nerve net or how the cells communicate with each other. Likewise, while extensive EM studies have provided high-resolution images of individual nerve cells, neurites, and synapses (Kinnamon and, 1981; Kinnamon and Westfall, 1982; Westfall, 1973; Westfall et al., 1971; Westfall et al., 1983), they could not reveal the overall organization of the nerve net.

The *Hydra* nerve net is unique in that it grows continuously. All *Hydra* tissues, including the nerve net, are newly formed every 2-3 weeks in well-fed animals (Campbell, 1967; David and Campbell, 1972; David and Gierer, 1974). Since cell proliferation occurs exclusively in the body column, there is continuous displacement of cells from the body column toward the head and foot and loss of cells at the extremities. In the course of this growth and displacement, the nerve net expands by the addition of nerve cells, which arise by differentiation from interstitial stem cells in the body column. Head- and foot-specific nerve cells are also continually added to these differentiated tissues. For example, tentacle tissue is completely renewed in 4-5 days by displacement of epithelial tissue from the body column into the tentacles. Ectodermal epithelial cells at the base of a tentacle differentiate into battery cells with the incorporation of nematocytes and newly differentiated sensory nerve cells (Hobmayer et al., 1990b).

In the present experiments, we take advantage of a newly developed pan-neuronal antibody (PNab), which stains all nerve cells and nerve processes in fixed *Hydra* polyps. Antibody staining and confocal microscopy show that nerve cells in *Hydra* are organized as two separate nerve nets, one in the ectoderm and one in the endoderm. Transmission electron microscopy (TEM) and block face scanning electron microscopy demonstrate that the two nerve nets consist of discrete bundles of overlapping nerve cell processes. The bundles include different nerve cell types and neural circuits. Cell type specific expression of innexins and formation of gap junctions provides the necessary circuit specificity. Strikingly, these neurite bundles extend past nerve cell bodies and do not appear to terminate on them. These results suggest a novel model for growth of the nerve net based on the lateral addition of new nerve cells to the existing net. We

confirmed this model by tracking the addition of newly differentiated nerve cells to the nerve net.

Results

A new peptide antibody stains the entire nerve net in *Hydra*

A rabbit antibody made against the peptide sequence VTRNQQDQQENRFSNQ (see Materials and Methods) stains the nerve net in *Hydra* and is referred to here as pan-neuronal antibody PNab (Figs. 1-3). In order to determine whether PNab recognizes all nerve cells in *Hydra*, two sets of experiments were performed. First, we investigated transgenic strains of *Hydra*, which express NeonGreen or GFP in nerve cells. One transgenic strain uses the promoter of an alpha-tubulin gene driving expression of NeonGreen. This transgene has been demonstrated to be strongly expressed in all differentiated nerve cells in *Hydra*, and correspondingly the entire nervous system is brightly NeonGreen-positive (Primak et al 2023). Fixed polyps of this strain were stained with PNab and transgenic NeonGreen expressing nerve cells were scored for PNab staining (see Materials and Methods). All NeonGreen-expressing nerve cells (684/684) were stained with PNab.

We also scored smaller numbers of PNab-stained nerve cells in two additional transgenic lines, i.e. Hym176B (Noro et al., 2019) and nGreen (see Materials and Methods). In the Hym176B line 149/149 transgenic nerve cells were stained with PNab. In the nGreen line 51/51 transgenic nerve cells were stained with PNab. We conclude from these results that PNab stains all nerve cells in *Hydra* and hence permits imaging of the entire nerve net.

In a second set of experiments we compared the number of PNab-stained nerve cells in confocal image stacks with the number of nerve cells determined by maceration of the same tissue (see Materials and Methods). Both measurements yielded a ratio of 0.12 nerve cells/epithelial cell (Suppl. Fig. 2C) confirming that PNab is a pan-neuronal marker staining all nerve cells in *Hydra*.

Imaging the *Hydra* nerve net with PNab

Figure 1A shows a low magnification confocal image of the upper body column of *Hydra* stained with PNab, including the hypostome and tentacles. The image shows primarily the ectodermal nerve net; endodermal nerve cells lie below the focal plane. The antibody stains both nerve cell bodies and nerve cell processes, which are oriented parallel to the oral-aboral axis of the body column and also extend into the tentacles. The hypostome forms a dome above the tentacle ring and includes nerve cells oriented toward the mouth opening in the center of the hypostome. Figure 1B shows a confocal image of the lower half of a body column. Ectodermal nerve processes are oriented along the oral-aboral axis but become less oriented in the peduncle. There is an increase in nerve cell numbers in a band just above the basal disk. Confocal images of “inverse

watermelon" polyps in Supplemental Figure 1 show the tissue structure in which the nerve net is embedded.

Figures 2A and B show a ring cut from the body column in the mid-gastric region with the ectodermal and endodermal nerve nets. The view is down the oral-aboral axis and the position of the mesoglea is shown as a green line for orientation (see also Suppl. Fig. 1C). The ectodermal nerve net consists of ganglion cells oriented along the oral-aboral axis and hence cut in cross section. The endodermal nerve net consists of roughly equal numbers of sensory cells and ganglion cells. The ganglion cells form a network near the base of endodermal cells whereas the sensory cells extend prominently up through the endodermal layer into the gastric cavity. Figures 2C and D show images from a single confocal stack taken through the body wall in the gastric region. Nerve cells in the ectoderm form an array of parallel processes oriented along the oral-aboral axis (Fig. 2C); those in the endoderm form a roughly polygonal array (Fig. 2D). Both nerve cell bodies and nerve cell processes stain with the PNab. The nerve cell bodies are roughly 10 µm long; the distance between nerve cell bodies is variable in both ectoderm and endoderm but usually 50-100 µm. While cell bodies and processes in the ectoderm are organized in a plane, which includes the muscle processes of the ectodermal cells, those in the endoderm are not closely associated with endodermal muscle processes (see below). Endodermal sensory cells extend deeper into the tissue (see Fig. 2B) and are not included in the image.

Higher magnification images (Fig. 3) of the hypostome, a tentacle, and the peduncle/basal disk reveal specific neuronal patterns with a higher density of nerve cells. Fig. 3B is a surface view of the hypostome showing a dense network of ganglion cells with nerve processes extending down the body column. Fig. 3C shows a section deeper in the hypostome roughly passing through the mouth opening. Sensory cells are prominent in the ectoderm near the mouth and extend to the outer surface of the tissue (Fig. 3B and C, red arrows). When viewed from above, these sensory nerve cells form a ring around the mouth opening (Fig. 3D red arrows). Sensory cells in the endoderm (Fig. 3C, yellow arrows) lie between the dense mass of mucous cells and endodermal epithelial cells, which make up the endodermal layer of the hypostome (see Suppl Fig 1A and B). They are connected to a network of ganglion cells in the endoderm under the mesoglea.

Fig 3E shows a surface view of a portion of an extended tentacle. Nerve cells form a roughly polygonal pattern associated with the battery cells, which form the ectoderm in tentacles. Single sensory nerve cells (Nv-1 positive; Hobmayer et al., 1990b) are integrated within battery cell complexes (Cramer von Laue, 2003; Hobmayer et al., 1990b). In the peduncle (Fig 3F) there is a broad band of increased nerve cell density, which is formed by a unique population of unusually large ganglion nerve cells. These cells stain strongly with PNab and have been shown to express the gap junction protein innexin 2 (Takaku et al., 2014), and the neuropeptides Hym 176A and RFa-A (Noro et al., 2019).

The nerve nets in the ectoderm and endoderm are separate structures and are differently associated with muscle processes

While the images in Figure 1-3 describe the complete nerve net, they do not permit localization of nerve cells or portions of the nerve net clearly to the ectoderm or the endoderm. To resolve this question, we used transgenic lines expressing Lifeact-GFP (Aufschnaiter et al., 2017), which binds specifically to filamentous actin (Riedl et al., 2008). Since most filamentous actin is concentrated in the muscle processes at the base of epithelial cells, these structures are brightly fluorescent in confocal images. The muscle processes are localized at the base of epithelial cells directly apposed to the mesoglea. Thus, they precisely mark the boundary between ectoderm and mesoglea and between endoderm and mesoglea.

Figure 4 shows segments of rings of body column tissue (see Fig. 2A) cut from an ectodermal Lifeact animal (Fig 4A) and from an endodermal Lifeact animal (Fig. 4B). In Figure 4A the green spots represent muscle fibers in the ectoderm, which run parallel to the oral-aboral axis of *Hydra*, and were cut when the ring was excised from the body column. The irregular red dots in between muscle fibers in the ectoderm are nerve cell processes. They are typically closely associated with muscle processes in the ectoderm. Underneath the ectodermal muscle processes there is a black space representing the mesoglea, which separates the ectoderm from the endoderm. Red PNab stained nerve cell bodies and neurites are also present in the endoderm.

Figure 4B shows the opposite situation in an endodermal Lifeact animal. Muscle processes at the base of endodermal epithelial cells are oriented circumferentially around the body column and mark the endodermal side of the mesoglea. An endodermal ganglion cell is stained by PNab and neurites from this cell extend parallel to but are separated from the muscle fibers. Thus there is a clear difference in the way the ectodermal and endodermal nerve nets are associated with muscle processes. The diagram in Fig. 4C shows this schematically. The localization of ectodermal ganglion cells completely overlaps the localization of ectodermal muscle processes. By contrast the localization of endodermal ganglion cells is largely separated from endodermal muscle processes.

Importantly, in Fig 4A and 4B there are no connections between nerve cells in the ectoderm and nerve cells in the endoderm. To search more extensively for nerve cell contacts between the ectoderm and endoderm, we imaged complete rings of body column tissue (see Fig. 2B) from 4 different PNab-stained Lifeact polyps. These rings contained a total of 133 nerve cells (57 ectoderm, 76 endoderm) and associated neurites and represented about 4% of the body column tissue. No contacts between the ectodermal and endodermal nerve nets were observed. We have taken many more image stacks at different positions in the body column, peduncle, and hypostome and never found a connection between the ectodermal and endodermal nerve nets.

There are no nerve cells in the endoderm of tentacles

In his original description of the *Hydra* nerve net, Hadži (1909) noted that nerve cells were not present in the endoderm of tentacles (Hadži, 1909). We have confirmed this unexpected result using PNab staining of Lifeact animals.

Figure 5A shows an image of the ectoderm at the base of the tentacles in an ectodermal Lifeact animal. The PNab stained nerve net lies above the green muscle processes of the ectodermal epithelial cells. The muscle processes are oriented parallel to the oral-aboral axis of the polyp and extend into the base of the tentacle. An image taken deeper in the tissue, below the ectodermal muscle processes (Fig. 5B), reveals PNab-stained nerve cells in the endoderm of the body column but no nerve cells in the endoderm of the tentacles. We also made image stacks through tentacles of endodermal Lifeact animals stained with PNab (Fig. 5C and D). There are many red nerve cells in the ectoderm above the green muscle processes (Fig. 5C), but no nerve cells in the endoderm below the muscle processes (Fig. 5D).

The absence of neurons in the tentacle endoderm indicates a massive loss of endodermal nerve cells during formation of tentacle tissue from tissue of the upper body column. We suggest that this loss of endodermal neurons is related to the formation of battery cells in the ectoderm (Hobmayer et al., 1990b) and reflects a remodeling of both the ectoderm and endoderm during tentacle formation.

Nerve cell numbers in the ectoderm and endoderm along the body column

Images of the nerve net in Figures 1-3 show only small differences in the apparent density of nerve cells along the body column. To put this qualitative observation on a quantitative basis, we counted nerve cells and epithelial cells in confocal image stacks through the body wall at various positions along the body column from the hypostome and tentacles to the basal disk. The results are shown in Figure 6. Most strikingly, there were no nerve cells in the endoderm of tentacles (see above). Similarly, the basal disk had very few nerve cells in the endoderm. In contrast to these two differentiated structures, the density of nerve cells in the body column endoderm is relatively constant (0.10-0.19) from the hypostome to the peduncle. The density of nerve cells in the ectoderm, however, changes dramatically along the body column. While the ratio of nerve to epithelial cells is relatively constant (0.15-0.22) in the gastric region and the peduncle, the number of nerve cells in the ectoderm rises sharply in the hypostome, tentacles and basal disk. These are regions known to have a high level of new nerve cell differentiation (see Discussion).

The nerve net consists of closely associated parallel tracks of neurites (bundles)

The images in Figures 1-3 do not reveal how the nerve net is constructed, i.e. how the size and shape of individual nerve cells contribute to the overall structure of the net. Do the connections between nerve cells in the net consist of overlapping neurites from neighboring cells or single neurites extending from one cell and synapsing on the next cell? To acquire such information, we stained transgenic nGreen polyps with PNab. This strain is a mosaic, in which not all stem cell precursors are transgenic. As a consequence, in a population of nGreen animals some polyps contain more and some fewer GFP-labeled nerve cells. We took advantage of this mosaicism to identify animals with relatively few GFP-labeled nerve cells. This allowed us to find isolated GFP-labeled nerve cells and thus image how such an individual nerve cell contributes to the PNab-stained nerve net.

Figure 7 shows two GFP-labeled nerve cells in the ectoderm with long neurites extending parallel to the body axis. The nGreen neurites (Fig 7A) are so closely associated with red PNab stained neurites (Fig. 7B) that it is almost impossible to distinguish the two. Only occasionally were the green or red neurites locally separated from each other so that both were visible (Fig. 7C). This showed that over long stretches the nerve net consists of bundles of neurites running parallel to each other.

The occurrence of bundles of parallel neurites suggests that a neurite from one cell may not only extend along the neurite of a neighboring cell, but also past the cell body of that neighboring cell. We have found numerous examples of such cell bodies in high-resolution confocal images. Figure 8 shows an example in which a red PNab-stained neurite passes next to a green GFP-labelled nerve cell body (Fig. 8A-C). A single optical section (Fig. 8 D-F) shows clearly that both the GFP-labeled and unlabeled neurites are stained with PNab. We also found examples in PNab stained preparations in which several tracks of neurites passed over a nerve cell body. In contrast to the above situation, we found few examples of neurites ending on the cell body of a neighboring cell. The ends of GFP-labeled neurites usually lie somewhere along the nerve net at a site that was otherwise unremarkable (see asterisks in Fig. 7C). Thus, communication along the nerve net appears to be a case of cell-to-cell communication by neurites interacting laterally to transmit a signal.

Electron microscopy confirms the widespread occurrence of neurite bundles

We sought to confirm the unexpected and widespread occurrence of neurite bundles by transmission electron microscopy (TEM). *Hydra* polyps were fixed and stained for TEM and sectioned perpendicular to the body axis. Figure 9A is a low magnification image of the ectoderm in the middle of the body column showing both the apical surface and the basal muscle fibers (green) of the epithelial cells lying directly over the mesoglea (yellow). The muscle processes are cut in cross-section and form a continuous mat immediately adjacent to the mesoglea. A bundle of four neurites lies next to a nerve cell body (ncb, red) and a second bundle with three neurites lies to the left of the nerve cell body. Both neurite bundles are directly adjacent to muscle processes in agreement with the PNab-stained image in Figure 4A. Figure 9B shows a higher magnification image of another bundle of 4 neurites in the ectoderm. The neurites contain numerous darkly stained glycogen granules and dense core vesicles, which are typically found in nerve cells (Westfall, 1973).

In addition, we used TEM cross-sections in the mid-body column to measure the frequency of neurite bundles with different numbers of neurites in a bundle. In the ectodermal nerve net, only about 20 percent of the cross-sectioned nerve tracks occurred as single neurites (Fig. 9C). About 80 percent of the nerve tracks occurred as bundles, many as bundles of 2 neurites, but often also as bundles consisting of 3-5 neurites (Fig. 9C).

Figure 9D shows a TEM cross-section of the endoderm in the middle of the body column with the basal muscle processes (green) directly adjacent to the mesoglea (yellow). Two major differences in nervous system architecture were obvious when endoderm was

compared with ectoderm. First, endodermal neurites and neurite bundles, containing numerous dense core vesicles, were located at some distance from the endodermal muscle processes (Fig. 9D, 9D'), equivalent to the findings obtained with PNab staining in confocal images (Fig. 4B). Second, about half of the endodermal nerve tracks were single neurites, the other half were bundles containing two neurites (Fig. 9C). Bundles with more than two neurites were not found in the endoderm. Thus, in summary, the ectodermal nerve net is more directly associated with muscle processes and clearly exhibits higher connectivity than the endodermal nerve net.

To extend the TEM results, we analyzed two thousand serial sections of the ectodermal epithelium in the mid-body region. Serial sectioning was carried out with the block face SEM method. Fig. 10A shows a 3D reconstruction of the serial sections. The imaged block is 56 x 40 x 13 µm and includes two nerve cell bodies and corresponding parallel tracks of neurites (purple and green) lying adjacent to muscle processes of the ectodermal epithelial cells. Neurites from three additional nerve cells (turquoise, yellow and red) whose cell bodies lie outside the sectioned block run parallel to and are closely associated with the neurites from the two nerve cells shown. The 3D reconstruction confirms at high resolution that nerve tracks between nerve cell bodies consist of bundles of two or more tightly associated nerve processes. The distance between the two nerve cell bodies along the oral-aboral axis is roughly 50 µm, in agreement with the distribution of nerve cell bodies shown in Fig. 2C and Suppl. Fig. 2A.

A striking feature of the reconstruction in Fig. 10A are neurites which run past the two nerve cell bodies (blue, purple and green). This result is in agreement with the images in Fig. 7, 8, and 9A, which also show neurites running past neighboring nerve cell bodies. While closely attached to these nerve cell bodies, the neurites do not appear to terminate on them. Fig. 10B and C are views from above and below the reconstruction taken from an interactive 3D model showing only the nerve cells and neurites (Suppl Fig 4). The blue, green and purple neurites extend over the entire length of the reconstructed block parallel to the long axis. By comparison, the yellow and red neurites meet in the middle and form thin terminal fingers, which overlap at the contact site for about 8 µm. The yellow neurite also forms a thin finger, which appears to contact a spur of the purple neurite for about 4 µm (Fig. 10C). Thus there are two qualitatively different connections between neurites: short, thin, overlapping regions, which suggest contact, and long parallel tracks apparently without contact. The short spur of the purple neurite (Fig 10C) contacts a muscle process.

Neurite bundles and neural circuits

The occurrence of neurite bundles raises questions of which nerve cell types and nerve circuits are involved. Based on the *Hydra* single cell atlas, there is only one ganglion nerve cell population in the endoderm (en1), and this population forms the endodermal nerve net (Cazet et al 2023). En1 corresponds to the endodermal neural circuit RP2 (Dupre and Yuste, 2017). By comparison there are two nerve cell populations (ec1/ec5 and ec3), which form the nerve net in the ectoderm. These two populations correspond to the contraction burst CB and RP1 neural circuits in the ectoderm (Dupre and Yuste, 2017; Giez et al, 2023a).

To visualize how ec1/ec5 and ec3 nerve cells contribute to nerve bundles in the ectodermal nerve net, we stained a Hym176B transgenic line (Noro et al, 2019), which expresses GFP in ec1 nerve cells in the hypostome and body column, with PNab, which stains all nerve cells. Figure 11A shows that Hym176B nerve cells form a continuous nerve net in the hypostome and body column. There are no Hym176B cells in the tentacles. The Hym176B cells are also stained with PNab. Parallel to the Hym176B nerve net there are additional nerve cells stained only with PNab. These are ec3 nerve cells. At higher magnification (Fig 11B) it is clear that both ec1 and ec3 nerve cells are closely associated in neurite bundles. Since these two ganglion nerve cell populations correspond to the two different neural circuits CB and RP1, neurites in the bundles need to form specific synaptic connections with the corresponding nerve cell type. As shown below, circuit-specific gap junctions provide the necessary specificity.

Neurites in bundles are linked by circuit-specific gap junctions

The TEM and block face images in Fig 9 and 10 do not have sufficient resolution to identify chemical synapses or gap junctions between neurites in bundles. To determine how neurites in bundles communicate with each other we used higher resolution TEM images on longitudinal sections of the ectoderm. Fig 12A and B show two examples of gap junctions between neurites in bundles. Detecting gap junctions by block face SEM or TEM is however difficult and it is not possible to determine which neural circuits are involved. Alternatively, scRNAseq results can now be used to detect innexin transcripts and reveal which cell types contain them. Innexins have been shown to form gap junctions in *Hydra* (Alexopoulos et al., 2004; Takaku et al., 2014) and a search of an updated scRNAseq database for *Hydra* (Cazet et al., 2023) has revealed that the two nerve cell populations constituting the CB and RP1 circuits in the ectoderm (Dupre and Yuste, 2017), each contain distinct innexin transcripts. The corresponding UMAPs are shown in Fig 12C. Both ec1 and ec5 nerve cells, which form the CB neural circuit, express innexin 2; ec3 nerve cells, which form the RP1 neural circuit, express innexins 6 and 14 (Fig 12C). Hence circuit specific gap junctions can be formed by innexins uniquely expressed in nerve cells of each circuit. Innexin 2 is also expressed in en1 nerve cells (Fig 12C), which form the RP2 circuit in the endoderm. There is, however, no cross-correlation between the neural activity profiles of CB and RP2 and RP1 and RP2 indicating that the endodermal and ectodermal neural circuits are not connected (Dupre and Yuste, 2017).

Nerve net growth occurs by lateral addition of new nerve cells to bundles

A unique feature of the *Hydra* nerve net is that it is a dynamic structure. It grows and is modified continuously. Since adult polyps do not increase in size, excess tissue generated by cell division is displaced into buds and to the ends of the body column (Campbell, 1967). Tentacle tissue is continuously renewed by differentiation of battery cells at the base of tentacles. Basal disk tissue is similarly renewed. Cells are lost by sloughing from the tips of the tentacles and the center of the basal disk. How new nerve cells are added to the nerve net was not known. The occurrence of bundles, however, suggests a simple way to add nerve cells to the net, by lateral association. Indeed, the

image in Figure 7 of two GFP-labeled nerve cells laterally associated with the PNab stained nerve net supports a model of nerve net growth by lateral addition.

To investigate how new nerve precursors are added to the nerve net we grafted unlabeled AEP polyps to transgenic nGreen polyps (Fig 13A). GFP-labeled nerve cell precursors migrated from the bottom half to the top half of such grafts and differentiated into new nerve cells. To localize the sites of new differentiation relative to the nerve net, we stained the grafts with PNab on day 1, 2 and 3 after grafting. Fig. 13B and C show images of young nerve cells (nGreen) associating with the nerve net (red) on day 2. Migrating precursors without neurites do not associate with the nerve net and most differentiating nerve cells with short neurites on Day1 were also not associated with the nerve net (Fig 13D). However, by Day 2 and 3 most differentiating nerve cells extended neurites along the nerve net (Fig 13D). The results suggest that outgrowing neurites actively seek lateral associations with the neurites of the existing nerve net.

Discussion

There are two separate nerve nets in *Hydra*: implications for motor control and contractile activity

PNab staining has permitted, for the first time, detailed imaging of the entire nerve net in *Hydra*. The results reveal two separate nerve nets, a net of interconnected nerve cells spread throughout the ectoderm and a second nerve net in the endoderm. There are no nerve cells in the endoderm of tentacles (Fig 5) and very few in the endoderm of the basal disk (Fig 6). No connections between the two nerve nets were found based on PNab staining of ectodermal and endodermal nerve cells in rings cut from the body column of four animals (see Results). This is in agreement with earlier TEM observations (Hufnagel and Kass-Simon, 1976). It also agrees with neural activity measurements showing no cross-correlation between firing patterns of the ectodermal CB and RP1 neural circuits and the endodermal RP2 neural circuit (Dupre and Yuste, 2017).

In the ectoderm, nerve cell bodies and nerve cell processes are closely associated with muscle processes at the base of ectodermal epithelial cells (Fig 4A and C). TEM images of cross-sections of the body column confirm the close association of nerve cells with muscle processes in the ectoderm (Fig 9, 10). This close association is consistent with direct neural control of body column contractions (see below). The localization of the endodermal nerve net is quite different. Endodermal nerve cells and their processes are located in a diffuse band at some distance from the endodermal muscle processes (Fig 4B and C; Fig 9D). Furthermore the polygonal pattern of endodermal nerve cells (Fig 2D) is completely different from the parallel array of endodermal muscle processes arranged circumferentially around the body column (Fig 4B). Both results suggest that the endodermal nerve net is not directly involved in controlling the activity of endodermal muscle processes.

Recently, Dupre and Yuste (2017) described electrical activity in nerve cells in a transgenic strain of *Hydra* that expresses the calcium reporter GCaMP6s in nerve cells

(Dupre and Yuste, 2017). They identified three discrete non-overlapping populations of nerve cells based on activity profiles (CB, RP1, RP2). Cells in each population fired together and there was no overlap between the firing patterns. The RP2 population was located in the endoderm, while the RP1 and CB populations were located in the ectoderm. The activity of the CB network was directly correlated with rapid contraction of the body column. The activity of the RP1 and RP2 networks was associated with slower changes in behavior.

The RP2 population is identical with the endodermal nerve net identified by PNab staining (Fig 2D; Fig 4B). Moreover, there are no RP2 nerve cells in the tentacles, in agreement with the absence of endodermal nerve cells in the tentacles as assayed by PNab staining (Fig 5). The observation that the RP2 nerve net is not associated with rapid changes in behavior is consistent with the limited contact between the endodermal nerve net and endodermal muscle processes (Fig 4B and 9D). However, endodermal ganglion cells do strongly express several neuropeptides, e.g. GLWa (Cazet et al., 2023; Siebert et al., 2019) and release of such neuropeptides could modulate contractile activity in endodermal muscle processes. In particular Takahashi et al. (2003) have shown that GLWa induces slow contraction of the endoderm and consequently elongation of the body column (Takahashi et al., 2003).

The two ectodermal circuits (RP1 and CB) (Dupre and Yuste, 2017) correspond to the ectodermal nerve net identified by PNab staining (Fig 2C and 4A). Although the nerve net in the ectoderm appears to be homogeneous, the results of scRNAseq experiments indicate that it consists of two populations of ganglion cells, which express distinct neuropeptides (Cazet et al., 2023; Siebert et al., 2019). Ec1 and Ec1/5 express the neuropeptide Hym176 (Noro et al., 2019) while Ec3 nerve cells express the neuropeptide GLWa.

To correlate neural activity with muscle activity, transgenic *Hydra* that express distinct calcium reporters in ectodermal and ectodermal epithelial cells were made (Szymanski and Yuste, 2019). This enabled detection of muscle activity in each epithelium during fast contraction of the body column initiated by CB nerve cells. The results showed that both ectodermal and endodermal epithelial cells responded simultaneously to activity of the CB circuit. Since there are no nerve cell connections between the ectoderm and the endoderm (see above), they postulated (Wang et al., 2023) that the ectodermal epitheliomuscle cells activate endodermal epitheliomuscle cells directly via gap junction connections across the mesoglea (Hand and Gobel, 1972). This conclusion is consistent with our findings. Nerve cells in the ectoderm are closely associated with ectodermal muscle processes (Fig 4A, 9 and 10) and TEM studies have described both chemical synapses and gap junctions between nerve cells and ectodermal muscle processes (Westfall, 1973; Westfall et al., 1971; Westfall et al., 1980). By comparison, our results indicate that such contacts are rare in the endoderm (Fig 4B and 9D) and there is no endodermal neural activity associated with the fast contraction of the body column (Dupre and Yuste, 2017).

The *Hydra* nerve nets consist of bundles of parallel nerve processes linked by circuit-specific gap junctions

Prior to the present results, it was not clear how the nerve net in *Hydra* is constructed. One possibility was that nerve processes from neighboring cells simply meet and synapse "end-to-end" or that a neurite from one cell synapses on the cell body of a neighboring nerve cell, as is the case in bilaterian nervous systems. Figures 7 and 8 show that, surprisingly, this is not the case. The connections between nerve cells along the body column mainly consist of two or more neurites attaching laterally to form bundles in the ectoderm (Fig. 9C). The EM images in Fig 9 and 10 confirm that neurites in such bundles are closely associated and show in addition that neurites in bundles extend past neighboring nerve cell bodies. Furthermore, the images of the nerve net in transgenic Hym176B polyps (Fig. 11) demonstrate that neurites in bundles in the ectoderm belong to two different neural circuits CB and RP1. Hence nerve cell-specific connections are required to carry circuit-specific signals. Circuit-specific gap junctions between neurites in bundles (Fig. 12A, B, C) appear to provide the necessary specificity. Furthermore, this result is consistent with the observation of Dupre and Yuste (2017) that nerve cells in the CB, RP1 and RP2 circuits fire simultaneously indicating that they are linked by gap junctions.

Earlier TEM studies have identified both chemical synapses and electrical synapses (gap junctions) between nerve cells and between nerve cells and epithelial cells in *Hydra* (Kinnamon and Westfall, 1981; Kinnamon and Westfall, 1982; Westfall et al., 1971; Westfall et al., 1980). These synapses occurred at multiple sites along neurites, so-called en passant synapses (Westfall et al., 1971), but were not associated with neurite bundles. The only previously described occurrence of neurite bundles was a "nerve ring" surrounding the hypostome in *Hydra oligactis* (Koizumi, 2007). This nerve ring contained 20-30 nerve cells (Koizumi et al., 1992) and TEM images of the nerve ring (Matsuno and Kageyama, 1984) showed that neurites and nerve cell bodies were tightly associated, similar to what is seen in the images in Fig 9 and 10.

Nerve cells and polyp form

The body column of *Hydra* is a tube formed by two sheets of epithelial cells separated by a basement membrane (mesoglea). The tube is closed at the basal end by the basal disk and at the apical end by the mouth. The epithelial cells have muscle processes abutting the mesoglea. The muscle processes of endodermal cells are arranged circumferentially around the body column (Fig 4B); muscle processes of ectodermal cells are arranged longitudinally, parallel to the oral/aboral axis (Fig 4A). The combined force of these two muscle sheets gives rise to the tubular shape of the body column.

In addition to muscle tension, the shape and behavior of the body column is affected by osmotic pressure. *Hydra* polyps live in fresh water and there is a constant influx of water into the cytoplasm of the epithelial cells. This water is transferred to the gastric cavity and periodically voided through the mouth (Benos and Prusch, 1972; Benos and Prusch, 1973; Yamamoto and Yuste, 2020) and potentially through the pore in the center of the basal disc (Shimizu et al., 2007).

The nerve cells in the two epithelial layers affect the dynamic behavior of this system. This is clearly seen in nerve-free *Hydra* (Campbell, 1976; Marcum and Campbell, 1978). These animals no longer contract and are nearly motionless due to the absence of

ectodermal nerve cells. The body column of nerve-free animals is also distended by increased osmotic pressure, which cannot be released through the closed mouth. However, regular experimental opening of the closed mouth in nerve-free animals leads to release of the gastric fluid and a return to normal tubular morphology of the body column (Wanek et al., 1980). Thus, one function of nerve cells in the endoderm is the control of endodermal muscle tension in response to osmotic pressure.

A role for the endodermal nerve net in feeding?

A striking feature of the endodermal nerve net is the large proportion of sensory cells, which constitute >50% of all endodermal nerve cells. These cells are oriented toward the gastric cavity (Fig 2B) and have sensory cilia, which extend into the gastric cavity to monitor digestive activity and perhaps also osmotic strength. They are connected to the ganglion network at their basal ends and could induce signals affecting changes in endodermal muscle processes associated with digestion. Two such events occur following ingestion of prey. First endodermal muscle processes below the tentacle ring contract locally ("neck formation") while endodermal muscles in the body column relax (Blanquet and Lenhoff, 1967). Together these events create a closed space in the gastric cavity for digestion of prey. After digestion is complete, slow contraction of endodermal muscle processes restores the normal columnar form of the body column.

Recent experiments of Giez et al (2023b) have now shown that endodermal ganglion cells are responsible for this regulation. These N4 nerve cells fire in response to swelling of the body column, e.g. when a food pellet is present in the gut. Ablation of N4 nerve cells using the nitroreductase-metronidazole (NTR-MTZ) system (Curado et al, 2007) prevents mouth opening and ejection of the food pellet, which leads to dramatic bursting of the gut. Expulsion of glass beads used as an artificial food pellet was also significantly delayed in N4 ablated animals. Hence endodermal ganglion cells are involved in regulating mouth opening and the swelling of the body column. The latter is a slow process, which could be caused by diffuse release of neuronal signaling molecules affecting muscle tension in endodermal muscle cells.

During digestion, slow waves of radial contraction move along the oral/aboral axis mixing the contents of the gut (Shimizu et al., 2004). Both neck formation and radial contractions are absent or strongly reduced in nerve-free animals consistent with a role for the endodermal nerve net in regulating digestion. The complete absence of nerve cells in the endoderm of the tentacles (Fig. 5), which are not involved in digestion, is consistent with this conclusion.

A model for continuous expansion of the nerve net in growing *Hydra* polyps

Hydra polyps grow continuously, but maintain a nearly constant size. The increasing cell numbers are displaced into buds, which develop in the lower body column and into the tentacles and the basal disk, which are terminally differentiated and continuously replaced by tissue from the body column (Campbell, 1967). As a consequence of this tissue growth, the *Hydra* nerve net undergoes continuous addition of new cells. This addition has been clearly shown in experiments tracking the differentiation of DiI-

labeled nerve precursors in live animals (Hager and David, 1997) or immigration of Brdu-labeled precursors (Technau and Holstein, 1996). Nerve cell differentiation occurred throughout the body column and maintained the constant ratio of nerve cells to epithelial cells (Fig 6).

The DiI experiments, however, could not visualize how newly differentiated nerve cells attached to the nerve net, since the nerve net was not labeled. The new experiment shown in Fig 13, in which the nerve net was imaged with the PNab antibody, demonstrates that new nerve cells are added laterally to the existing nerve net. Thus, the nerve net is an overlay of individual nerve cells and neurites as shown in Fig 7 and 8 and this overlay is a consequence of how it grows. Figure 14 summarizes these results in a simple model for growth of the nerve net. One consequence of this model is that elongating neurites terminate at apparently unspecific positions along a preexisting neurite track (Fig 7 and 10). A second consequence is that elongating neurites grow past neighboring nerve cell bodies (Fig 9A and 10). Both features are supported by our results and suggest that the existing nerve net acts as a template for the addition of new nerve cells.

Nerve cell differentiation in the hypostome, tentacles, and peduncle

The results in Fig 6 show that the nerve cell to epithelial cell ratio in the endoderm is nearly constant along the body column. As discussed above, this ratio can be maintained by continuous addition of new cells to the nerve net during growth. Similarly, in the ectoderm of the gastric region and the peduncle, the nearly constant ratio of nerve cells to epithelial cells can be maintained by addition of new cells to the existing nerve net.

The tentacles, hypostome, and basal disk, however, all contain increased numbers of nerve cells in the ectoderm (Fig 6) compared to the body column tissue from which they arise by tissue displacement. This implies new nerve cell differentiation in these tissues. This new differentiation has been well documented in earlier experiments (David and Gierer, 1974; Hager and David, 1997; Hobmayer et al., 1990a; Hobmayer et al., 1990b; Technau and Holstein, 1996; Yaross and Bode, 1978a; Yaross and Bode, 1978b) and is presumably associated with additional sensory and motor activities in these tissues. Indeed a fourth GCaMP6s activity pattern was identified in nerve cells at the base of tentacles (Dupre and Yuste, 2017), which was associated with movement of the head (nodding). A specific population of sensory nerve cells (Nv1) was identified which are incorporated into the battery cell complex in the ectoderm of tentacles (Hobmayer et al., 1990a; Hobmayer et al., 1990b). At the opposite end, in the lower peduncle, a population of nerve cells was identified, which express the *innexin2* gene (Takaku et al., 2014). Elimination of the activity of these gap junctions disrupted contractile activity of the body column. In all of these examples, it is possible to imagine that the lateral addition of new nerve cells to the existing nerve net (see Fig 14) gives rise to local changes in neural activity.

Finally, the nerve net is not just modified by addition as described above, but also by deletion of nerve cells. As shown in Figs 5 and 6, there are no nerve cells in the endoderm of the tentacles, even though this tissue arises by displacement of body column tissue, which contains nerve cells in the endoderm. This implies that nerve cells

in the endoderm are removed when endodermal tissue moves into tentacles. It appears likely that this occurs by apoptosis (Cikala et al., 1999), although this has not been observed directly. A similar process presumably removes nerve cells from endodermal tissue entering the basal disk. It also indicates a constant turnover of existing neuron-neuron and neuron-epithelial cell interactions. The molecules involved in the underlying feedback communication for these processes are currently unknown.

Materials and Methods

Animals

Hydra strains were maintained in laboratory cultures and fed 2-3 times per week with *Artemia* nauplii. *Hydra* medium (HM) contains 1 mM NaCl, 1 mM $CaCl_2$, 0.1 mM KCl, 0.1 mM $MgSO_4$, 1mM Tris (pH 7.6). The following strains were used for all experiments: *Hydra vulgaris* AEP (wildtype); transgenic strains: watermelon (expressing GFP and DsRed2 in ectodermal and endodermal epithelial cells respectively); inverse watermelon (expressing DsRed2 and GFP in ectodermal and endodermal epithelial cells respectively (Glauber et al., 2013); nGreen (expressing GFP in nerve cells, a few nests of differentiating nematocytes and gland cells; see below); Lifeact ecto (expressing Lifeact peptide-GFP fusion protein in ectodermal epithelial cells); Lifeact endo (expressing Lifeact peptide-GFP in endodermal epithelial cells) (Aufschnaiter et al., 2017); Hym176B (expressing GFP in a subpopulation of ectodemal nerve cells under control of the Hym176B promoter) (Noro et al 2019); alpha-tubulin pan-neuronal (expressing NeonGreen in all nerve cells under control of an alpha-tubulin promoter) (Primak et al 2023).

Generation of the nGreen transgenic line

The nGreen line was generated by microinjection of embryos from the SS1 strain of *Hydra vulgaris* AEP. SS1 is an F1 line that was generated by self-crossing of AEP. The plasmid pHyVec1 (GenBank accession number AY561434), which contains an actin promoter driving expression of GFP, was used for injection. Injection and screening of embryos was carried out as previously described (Wittlieb et al., 2006; Juliano et al., 2014). The nGreen line showed GFP expression in all types of nerve cells, a few nests of differentiating nematocytes and gland cells. The nGreen line used here is a mosaic containing both transgenic and non-transgenic interstitial stem cells. As a consequence, not all differentiated cells express GFP.

Counting cells by tissue maceration

Tissue maceration to identify and count *Hydra* cell types was carried out as previously described (David, 1973; Bode et al., 1973) with modifications. Maceration solution is composed of glycerol, glacial acetic acid, and water (1:1:13). Whole *Hydra* or tissue pieces were incubated in maceration solution for 10 minutes with gentle shaking to

dissociate the tissue. An equal volume of 8% PFA was added to fix the macerated cells. 50 µl of the suspension of macerated cells were spread evenly over about 2 cm^2 on a subbed microscope slide and dried. Two drops of glycerol:water (1:1) were added to the dried spread and covered with a cover slip. Nerve cells and epithelial cells were counted under a phase contrast microscope.

Counting nerve cells and epithelial cells in confocal image stacks

To count ectodermal and endodermal epithelial cells in confocal stacks, we used transgenic animals expressing GFP in the ectoderm and DsRed2 in the endoderm (watermelon line) or vice versa (inverse watermelon line). Since both DsRed2 and GFP are partially concentrated in the nuclei of transgenic epithelial cells, nuclei of epithelial cells can be distinguished from the DAPI stained nuclei of other cells. GFP nuclei are turquoise and DsRed2 nuclei are magenta (see Suppl Fig 1). The nuclei of all other cells are blue (DAPI). Suppl Fig 2B shows a confocal image stack in the ectoderm of a transgenic watermelon *Hydra* expressing GFP in ectodermal epithelial cells. The epithelial cell nuclei are clearly visible as round spots lying above the ectodermal muscle fibers oriented parallel to the body axis. Nerve cells stained with PNab in the same image stack are shown in Suppl Fig 2A. Yellow spots indicate nerve cell nuclei confirmed by DAPI staining.

Preparation and specificity of the PNab antibody

A rabbit antibody was generated against the peptide sequence VTRNQQDQQENRFSNQ, which corresponds to amino acids 4372-4388 in the cytoplasmic domain of the classic cadherin of *Hydra vulgaris (magnipapillata strain 105)* (GenBank accession number XP_012558722). Peptide synthesis, immunization of three rabbits, and subsequent isolation and purification of the IgG fraction were carried out by Dr. J. Pineda Antibody Service (Berlin). The resulting antibody was highly specific for nerve cells in *Hydra vulgaris* (Cramer von Laue, 2003; Bertulat, 2008). Pre-absorption with the synthetic peptide blocked antibody staining (Cramer von Laue, 2003).

Although PNab was made to a peptide in the classic cadherin of *Hydra vulgaris*, it is now clear that it does not recognize the cadherin protein. Both *Hydra oligactis* and *Hydra viridissima* have classic cadherin proteins and nerve cells in both of these species also stain strongly with PNab (Holstein, 2023). However, newly available cadherin gene sequences from *Hydra oligactis* and *Hydra viridissima* show that the sequences of the intracellular domain of classic cadherin differ dramatically between the three species (Suppl Fig 3). In particular the 18 amino acid sequence used to make the PNab antibody is only present in the *Hydra vulgaris* cadherin but not in the *Hydra oligactis* and *Hydra viridissima* cadherins. Hence, it is clear that PNab cannot be staining cadherin in neurons and the identity of the PNab antigen is presently unknown. Nevertheless PNab is a highly specific reagent to identify nerve cells in all species of *Hydra*.

Immunofluorescent staining of fixed *Hydra*

Immunofluorescent staining was performed based on a protocol optimized for double-labeling experiments with other polyclonal antibodies (Bertulat, 2008). Prior to fixation, animals were relaxed with 2% urethane in HM for a few minutes to prevent excessive contraction induced by fixation. Animals were fixed for 1 hour in 4% paraformaldehyde in PBS (120 mM NaCl, 50 mM K_2HPO_4, 12 mM NaH_2PO_4, pH 7.2-7.4). Following fixation animals were washed 3x in PBS. Animals used in Figure 8 were fixed with Lavdowsky's fixative (48% ethanol, 3.6% formaldehyde and 3.8% acetic acid in water).

To improve antibody access to all cells in the polyp, fixed animals were cut in half or into smaller pieces depending on the experiment. Cutting animals also enabled better mounting of body parts for imaging, e.g. top view of the hypostome or horizontal rings of the body column allowing views down the y-axis. Cutting was performed after fixation in order to maintain the structural features of the tissue, which was important for analysis of neuronal network characteristics.

Immunostaining was performed according to the following protocol. Fixed tissue was washed 3x in PBS, permeabilized in 0.5% Triton in PBS for 15 minutes, blocked for 20 minutes in 10 mg/ml bovine serum albumin (BSA), 0.1% Triton in PBS. Tissue pieces were incubated in primary antibody in blocking solution overnight at 4°C, then washed 3X in PBS and incubated in secondary antibody in blocking solution for 2 hours. Tissue fragments were then washed 3x in PBS (10 min), stained with DAPI (1 mg/ml) in PBS (10 minutes), and washed 1x in PBS.

Stained specimens were mounted on microscope slides with VECTASHIELD HardSet Antifade Mounting Medium. Bee wax was used on the edges of coverslip to prevent squashing of the preparations. Coverslips were sealed with nail polish and slides were stored at 4°C.

Primary and secondary antibodies used for staining, together with their respective dilutions, are listed below:
Primary antibodies: PNab (rabbit) 1/1000 (Thomas Holstein, Heidelberg); anti-GFP (chicken) 1/500 (Aves Lab).
Secondary antibodies: Alexa 488 donkey anti-chick 1/400 (Dianova 703-546-155); Cy3 donkey anti-mouse 1/200 (Dianova 715-166-151); Cy3 donkey anti-rabbit 1/400 (Dianova 711-165-152).

Confocal Imaging

Specimens were examined with a Leica SP5 scanning confocal microscope. Image stacks were taken with 10x, 20x and 63x objective lenses. Images at 10x and 20x magnification were taken every 1 µm. Images at 63x magnification were taken every 0.3 µm. Images were processed with ImageJ. The plugin StackGroom was used to correct z-shift and to create RGB stacks. Most images shown are maximum intensity projections of short stacks (5-15 µm).

Transmission Electron Microscopy (TEM) and Serial Block Face Imaging (SBFI)

Sample preparation was carried out according to a modified protocol of Deerink et al. (2010) adapted for *Hydra*. In brief, *Hydra* polyps were relaxed with 2% urethane in *Hydra* medium (HM) and immediately fixed with 2.5% glutaraldehyde in HM for 5 minutes, cut in half and further fixed for 2 hours. After washing in cacodylate buffer, samples were postfixed with ferrocyanide osmium tetroxide, treated with thiohydrocarbazide-osmium and in block stained with uranyl acetate and lead aspartate to enhance contrast. After dehydration with acetone, samples were infiltrated with increasing concentrations of acetone-resin and finally embedded in Durcupan ACM resin, mixture hard. The samples were oriented in small silicon molds and polymerized at 60°C for 48 h.

For TEM, ultra-thin sections were cut with an ultramicrotome UCT (Leica, Vienna) using a diamond knife (Diatome, Switzerland) and examined with an Energy Filter Transmission Electron Microscope Libra 120 (Zeiss, Germany). Images were acquired using a 2x2k high speed camera and an ImageSP software (Tröndle, Germany).

For serial block face imaging (SBFI), the resin block was mounted on a SEM stub with conductive glue, trimmed to 0.5 x 0.5 x 0.5 mm and coated with gold with a sputter coater. 3D imaging was performed on a FEI Quanta FEG 250 scanning electron microscope with an integrated ultramicrotome (prototype, workgroup W. Denk, MPI Neurobiology Munich) at 2.5kV. 2000 planes were cut in 30 nm steps at a lateral resolution of 20 x 20 nm, resulting in a volume of 40.5 x 13 x 60 µm. Neurites, nerve cell bodies, and nuclei were segmented and rendered using Amira® 5.6 software.

Acknowledgements

The authors thank Shawn Mikula of the Denk Lab at the Max Planck Institute for Neurobiology in Martinsried for help with block face sectioning, the Center for Advanced Light Microscopy (CALM) in the Biozentrum for access to confocal microscopes, Angelika Boettger for laboratory space and resources, Sigrid Grieser-Ade, Natalie Kolb, and Anne Kuhn for *Hydra* culture and Hermann Rohrer and Suat Özbek for discussions. The images in Fig 11 were generously provided by Amber Louwagie.

Author contributions

AK, SS, CB and OA did PNab imaging of *Hydra* tissue. CB did tissue transplantation and tracking of differentiating nerve precursors. CCvL and BB characterized PNab and did initial imaging. WS and MH did TEM imaging and 3D reconstruction of block face sections. KMG and RES made the transgenic *Hydra* strain nGreen. BH and TWH initiated the project at the Technical University of Darmstadt and made the PNab. BH, TWH and CND coordinated the research and wrote the paper.

Funding

AK, SS and CB were funded by the Masters Program at the Ludwig-Maximilians-University Munich. CCv (Technical University of Darmstadt) and BB (Technical

University of Darmstadt, Heidelberg University) were funded by grants from the Deutsche Forschungsgemeinschaft (DFG). WS and BH were funded by the Marie-Sklodowska-Curie COFUND program 847681 “ARDRE Ageing, Regeneration and Drug Research”. BH and TWH were funded by grants from the DFG (Ho1621/3 and SFB 474/B1). TWH was funded by grants from the DFG (Ho1088/2, SFB 269/A5, SFB 488/A12, and SFB 873/A1).

Figure Legends

Fig. 1: Distribution of PNab-stained nerve cells along the *Hydra* body axis. The confocal images are maximum intensity projections of short stacks (10-15 µm) showing the ectoderm. (A) Upper body column including the hypostome and tentacles. (B) Lower body column including the peduncle and basal disk. Scale bar: 150 µm.

Fig. 2: Distribution of PNab-stained nerve cells in a cross-section of the body column. (A) Schematic shows the position of imaged tissue. (B) Circular ring of tissue excised from the body column and viewed from above. The green line traces the position of the mesoglea separating ectoderm and endoderm except where tissue is compressed in the upper left quadrant. The ectodermal and endodermal nerve nets are separate structures. Red arrows indicate sensory cells extending from the endodermal ganglion net into the gastric cavity. (C and D) Maximum intensity projection images of short stacks through the body wall showing parallel tracks of neurites and nerve cell bodies in the ectoderm (C) and a polygonal pattern of nerve cells and neurites at the same position in the endoderm (D). Oral is to the top, aboral to the bottom. Scale bars: (B) 100 µm, (C and D) 30 µm.

Fig. 3: PNab-stained nerve cells in the hypostome (B, C, D), tentacle (E), and peduncle/basal disk (F). (A) Schematic shows the orientation of the confocal images. The images are maximum intensity projections of short stacks (10-15 µm) through the ectoderm of the hypostome (B) and deeper in the tissue at the same position (C) showing sensory nerve cells in the ectoderm (red arrows) and in the endoderm (yellow arrows). (D) Ectoderm surrounding the mouth opening viewed from above showing sensory nerve cells in ectoderm (red arrows). (E) Ectodermal nerve net in a short section of tentacle tissue. (F) Ectodermal nerve net in the peduncle and basal disk. Scale bars: (B, C, D, E and F) 30 µm.

Fig. 4: Segments of a ring of body column tissue excised perpendicular to the main body axis from Lifeact ecto (A) and Lifeact endo (B) polyps stained with PNab (red) and anti-GFP (green). The confocal images are maximum intensity projections of short stacks (20 µm) down the body column. (A) Lifeact ecto polyp. In the ectoderm small red spots (neurites) and green spots (muscle processes) alternate and are directly adjacent to the unstained mesoglea. In the endoderm neurites of ganglion cells are located at some distance from the mesoglea. Two sensory nerve cells (white arrows) in the endoderm extend upwards to the gastric cavity. (B) Lifeact endo polyp. Green muscle processes extend laterally in the plane of the image. The apical actin network of the endodermal cells faces the gastric cavity and is also strongly stained green (yellow arrow). A single ganglion cell in the endoderm extends red neurites parallel to, but separate from green muscle processes. (C) Schematic shows the position of ectodermal and endodermal nerve nets relative to corresponding muscle processes and the mesoglea. Scale bar: 30 µm.

Fig. 5: Lifeact ecto (A and B) and Lifeact endo (C and D) polyps stained with PNab. Confocal images are maximum intensity projections of image stacks in the ectoderm and endoderm. Small schematics indicate position of the images. (A) Lifeact ecto polyp showing the base of a tentacle. Green muscle processes extend parallel to the oral-aboral body axis and into the base of the tentacle. Red neurites are closely associated

with muscle processes and extend into the tentacle. (B) Image at the same position as (A) but deeper into the tissue showing absence of nerve cells in the endoderm of the tentacle but a nerve cell and neurites in the endoderm of body column (white arrow). (C) Lifeact endo polyp showing a tentacle surrounded by circular green muscle processes. Red nerve cells form a net in the ectoderm. (D) Same position but deeper in the tissue than (C), showing complete absence of red nerve cells in the endoderm. Scale bars: A and B: 30 µm; C and D: 100 µm.

Fig. 6: Nerve cell to epithelial cell ratio along the body column of *Hydra*. Transgenic watermelon and inverse watermelon polyps were stained with PNab to identify nerve cells and with DAPI to identify nuclei. Confocal stacks were taken through the body wall at various positions along the body column and scored for ectodermal and endodermal epithelial cells and for nerve cells (see Suppl Fig 2 and Methods). The results are semi-quantitative, since the number of animals scored (shown in brackets) and the number of image stacks varied at each position. A total of 80-400 nerve cells were scored in body column and peduncle samples, 20-30 in hypostome samples, but only 0-2 in the endoderm of tentacle and basal disk due to absence or very rare occurrence of endodermal nerve cells in these body parts.

Fig 7: Transgenic nGreen polyp stained with anti-GFP (green) and PNab (red). Confocal images of the ectoderm in the body column showing two GFP labeled nerve cells overlapping the PNab stained nerve net. (A) anti-GFP, (B) PNab and (C) overlay of anti-GFP (green) and PNab (red) images. White asterisks mark three GFP-labeled neurites, which run parallel to and terminate on the PNab-stained nerve net. Note that GFP-labeled nerve cells are also stained with PNab. Scale bar: 30 µm.

Fig. 8: Transgenic nGreen polyp stained with PNab (red) and anti-GFP (green). (A-C) Maximum intensity projection confocal image stack of a GFP-stained nerve cell tightly associated with an PNab (red) stained neurite from another cell. (D-F) Single optical section from the image stack in (A) showing parallel GFP and non-GFP neurites, both stained with PNab. The yellow arrowheads mark the outer boundary of the two parallel neurites in (D), (E) and (F). Scale bar: 5 µm.

Fig. 9: Position and structure of neurite bundles in the mid-body column in transmission electron microscopy (TEM) cross-sections. To facilitate identification, neurites are overlaid in orange-blue-purple, the nerve cell body in red, muscle processes in green, and the mesoglea in yellow. (A) Low magnification of the ectoderm. A nerve cell body (nvb) is directly associated with the muscle processes, and four neurites cut in cross section run parallel to the nerve cell body. An additional neurite bundle containing three neurites with contact to a muscle process is visible to the left of the nerve cell body. (B) Higher magnification image of another bundle of four neurites in contact with and running parallel to muscle processes. (C) Quantitative analysis of the relative amount of neurite bundle complexity using four TEM cross-sections spanning 40 µm in the mid-body column. Analysis included 130 nerve tracks in the ectoderm and 47 nerve tracks in the corresponding endodermal area. In the ectoderm, about 20% of nerve tracks consist of single neurites, about 80% of bundles contain 2-5 neurites. In contrast, about 50% of endodermal nerve tracks consist of single neurites, and about 50% contain two neurites. (D) Cross section of the endoderm showing a single neurite and a bundle with two neurites located at some distance to the basal muscle processes and

the mesoglea. (D') Higher magnification of the endodermal nerve bundle reveals numerous dense core vesicles and mitochondria.
Scale bars: (A) 10 µm; (B) and (D) 5 µm; (D') 2 µm.

Fig. 10: 3D reconstruction of 2000 serial sections obtained by serial block face SEM in the ectoderm of the body column. (A) Two nerve cell bodies and their neurites are colored green and purple (nuclei are highlighted in blue). Three additional neurites from nerve cells outside the imaged block are colored yellow, red and blue. The imaged block is 56 µm long. (B) and (C) Top and bottom projections from an interactive model of the reconstruction showing only nerve cell bodies and neurites (see Suppl Fig 4). Scale bars: 20 µm,.

Fig. 11: Nerve cell composition of nerve bundles. Transgenic Hym176B animal stained with anti-GFP and PNab. (A) Overview of hypostome (white arrow), tentacles and upper body column showing transgenic Hym176B nerve cells stained with anti-GFP (green) and all nerve cells stained with PNab (red). (B) High magnification image of the same Hym176B animal showing nerve cell bodies and neurite bundles in the nerve net. Most bundles consist of both Hym176B neurites and PNab stained neurites (stained only with PNab). Scale bars: (A) 150 µm; (B) 15 µm.

Fig. 12: Gap junctions and innexins. (A and B) TEM images of longitudinal sections in the mid-body column of the ectoderm show neurite bundles running along muscle processes. Gap junctions (black arrows) connecting two neurites (n) are indicated by arrow heads. To facilitate identification, muscle processes are overlaid in green and the mesoglea in yellow. Scale bar: 2 µm. (C) *Innexin* genes 2, 6, and 14 are uniquely expressed in specific nerve cell populations. UMAPs show expression (orange spots) of individual *innexin* genes in specific nerve cell populations: *innexin2* in Ec1/5 and Ec1 in the ectoderm and En1 in the endoderm; *innexin6* and *innexin14* in Ec3 in the ectoderm.. The UMAP identifying cell populations is shown as a gray background. Data from (Cazet et al., 2023).

Fig. 13: Differentiation of migrating nerve cell precursors in AEP(top)/nGreen(bottom) grafts stained with PNab. (A) Schematic of AEP/nGreen graft. (B and C) Two images of differentiating nerve cell precursors (nGreen) on Day 2 after grafting. Nerve net stained with PNab (red). White arrows mark association of nGreen neurites with the red nerve net. Differentiating nGreen nerve cells are stained with PNab and hence appear yellowish in the images. (D) Neurite outgrowth and association with the nerve net on Days 1-3 after grafting. Each spot represents one nGreen nerve cell. Scale bars: 15 µm.

Fig. 14: Schematic diagram of nerve net growth by lateral association of newly differentiated nerve cells (blue) with the pre-existing nerve net (green and red). Upper images: the base of tentacles; lower images: the middle of the body column. The images are approximately to scale and show changes associated with tissue growth. (A) Nerve net at t_0. (B) Nerve net during tissue growth. Lower image pair: new nerve cell (blue) attaches laterally to the nerve net (as shown in Fig 11) and thus maintains the ratio of nerve cells to epithelial cells during growth of the nerve net. Upper image pair: new nerve cell attaches laterally to the nerve net at the base of a tentacle. The nerve net does not grow at this position but is displaced into the tentacle. Newly differentiated nerve

cells thus increase the ratio of nerve cells to epithelial cells in the ectoderm of the tentacle (see Fig 6).

Supplementary Figure Legends

Suppl. Fig. 1: Structure of *Hydra* tissue imaged in transgenic polyps expressing DsRed2 in ectodermal epithelial cells and GFP in endodermal epithelial cells. Nuclei are stained with DAPI. Images are maximum intensity projections of short stacks (3-5 um). Ectodermal nuclei are magenta (DAPI + DsRed2). Endodermal nuclei are turquoise (DAPI + GFP). Blue DAPI nuclei are non-transgenic interstitial cell derivatives. (A) Hypostome, tentacles and upper body column. Vertical optical section through the mouth region. (B) High magnification image showing endodermal cells of the mouth opening extending to the surface of the hypostome. Extensive black spaces in the endoderm are occupied by mucous cells. (C) Segment of tissue ring excised from the body column showing ectoderm (red) on the outside and endoderm (green) on the inside. Black spaces are non-transgenic interstitial cell derivatives (gland cells in the endoderm, interstitial stem cells and nematoblast nests in the ectoderm). (D) Longitudinal optical section through a tentacle showing large endodermal cells in center flanked by red ectodermal (battery) cells containing embedded nematocytes (blue nuclei in black spaces). Scale bars: (A) 150 µm, (B, C, D): 30 µm.

Suppl. Fig. 2: Representative images of PNab stained body column of a transgenic watermelon polyp (GFP in ectoderm, DsRed2 in endoderm) used to count epithelial cells and nerve cells. The images are 250 x 250 µm. The stack depth is 20 µm. Such images were used to count nerve cells and epithelial cells in the ectoderm.
(A) PNab (red) stained nerve cells (nerve cell nuclei stained with DAPI are indicated by yellow spots). (B) anti-GFP (green) stained ectodermal epithelial cells; nuclei appear as round spots above parallel muscle processes at the base of the cells. Scale bar: 30 µm.
(C) Nerve to epithelial cell ratio assayed by maceration and by cell counting in confocal image stacks (see Methods). Three maceration preparations containing 8, 9, and 10 animals respectively were scored to yield an average value of 0.12 nerve cells per epithelial cell. Seven PNab stained *Hydra* were imaged by confocal microscopy. The ratio of nerve cells to epithelial cells in confocal image stacks taken through the body wall in the gastric region varied between animals; the average value was 0.12 nerve cells per epithelial cell.

Suppl. Fig. 3: Sequence alignment of the intracellular domains of classic cadherin proteins from *Hydra vulgaris* (strain 105), *Hydra oligactis* and *Hydra viridissima*. The p120/delta-catenin and the beta-catenin binding domains are highly conserved in all three species and anchor the alignment. The sequence between these two conserved domains is quite variable and, in particular, the 18 amino acid sequence (green) used to make the PNab antibody is only present in the *H. vulgaris* sequence.

Suppl. Fig. 4: 3D interactive model of the serial block face scanning SEM reconstruction shown in Fig 10. The interactive 3D model can be accessed by clicking into the Figure and dragging the image with the left mouse button pressed. (Adobe Reader Version 7 or higher required)

References

Alexopoulos, H., A. Bottger, S. Fischer, A. Levin, A. Wolf, T. Fujisawa, S. Hayakawa, T. Gojobori, J.A. Davies, C.N. David, and J.P. Bacon. 2004. Evolution of gap junctions: the missing link? *Current Biology* 14:R879-880.

Anderson, P.A. 1990. Evolution of the first nervous systems. Plenum Press.

Arendt, D., M.A, Tosches and H. Marlow. 2016. From nerve net to nerve ring, nerve cord and brain – evolution of the nervous system. *Nature Reviews Neuroscience*. 17:61-72.

Aufschnaiter, R., R. Wedlich-Soldner, X. Zhang, and B. Hobmayer. 2017. Apical and basal epitheliomuscular F-actin dynamics during *Hydra* bud evagination. *Biol Open* 6:1137-1148.

Benos, D.J., and R.D. Prusch. 1972. Osmoregulation in fresh-water *Hydra*. *Comparative Biochemistry and Physiology Part A: Physiology*. 43:165-171.

Benos, D.J., and R.D. Prusch. 1973. Osmoregulation in *Hydra*: Column contraction as a function of external osmolality. *Comparative Biochemistry and Physiology Part A: Physiology*. 44:1397-1400.

Bertulat, B. 2008. Identification and characterization of basic helix-loop-helix (bHLH) transcription factors in the context of the interstitial stem cell system of the freshwater polyp *Hydra*. Technical University of Darmstadt Darmstadt. 142.

Blanquet, R.S., and H.M. Lenhoff. 1967. Tyrosine enteroreceptor of *Hydra*: Its function in eliciting a behavior modification. *Science* 159: 633-634.

Bode, H., S. Berking, C.N. David, A. Gierer, H. Schaller, and E. Trenkner. 1973. Quantitative analysis of cell types during growth and morphogenesis in *Hydra*. *Wilhelm Roux Arch Entwickl Mech Org*. 171:269-285.

Bosch, T.C., A. Klimovich, T. Domazet-Loso, S. Grunder, T.W. Holstein, G. Jekely, D.J. Miller, A.P. Murillo-Rincon, F. Rentzsch, G.S. Richards, K. Schroder, U. Technau, and R. Yuste. 2017. Back to the Basics: Cnidarians Start to Fire. *Trends Neurosci*. 40:92-105.

Campbell, R.D. 1967. Tissue dynamics of steady state growth in *Hydra littoralis*. II. Patterns of tissue movement. *J Morphol*. 121:19-28.

Campbell, R.D. 1976. Elimination by *Hydra* interstitial and nerve cells by means of colchicine. *J Cell Sci*. 21:1-13.

Cazet, J.F., S. Siebert, H. Morris Little, P. Bertemes, A.S. Primack, P. Ladurner, M. Achrainer, M.T. Fredriksen, R.T. Moreland, S. Singh, S. Zhang, T.G. Wolfsberg, C.E. Schnitzler, A.D. Baxevanis, O. Simakov, B. Hobmayer, and C.E. Juliano. 2023. A chromosome-scale epigenetic map of the *Hydra* genome reveals conserved regulators of cell state. *Genome Res.* 33:283-298.

Cikala, M., B. Wilm, E. Hobmayer, A. Bottger, and C.N. David. 1999. Identification of caspases and apoptosis in the simple metazoan *Hydra*. *Current Biology*. 9:959-962.

Cramer von Laue, C. 2003. Analysis of the dual function of beta-Catenin in Wnt signaling and in Cadherin-mediated cell adhesion of *Hydra*. Technical University of Darmstadt, Darmstadt. 97.

Curado, S., Anderson, R.M., Jungblut, B., Mumm, J., Schroeter, E., and , D.Y. Stainier. 2007. Conditional targeted cell ablation in zebrafish: a new tool for regeneration studies. *Dev Dyn.* 236:1025-35.

David, C.N. 1973. A quantitative method for maceration of *Hydra* tissue. *Wilhelm Roux Arch. EntwMech. Org.* 171:259-268.

David, C.N., and R.D. Campbell. 1972. Cell cycle kinetics and development of *Hydra attenuata*. I. Epithelial cells. *J Cell Sci*. 11:557-568.

David, C.N., and A. Gierer. 1974. Cell cycle kinetics and development of *Hydra attenuata*. III. Nerve and nematocyte differentiation. *J Cell Sci*. 16:359-375.

Deerinck, T., E. Bushong, A. Thor, and M. Ellisman. 2010. NCMIR methods for 3D EM: A new protocol for preparation of biological specimens for serial block face scanning electron microscopy. *Microscopy* 1:6-8.

Dunne, J.F., L.C. Javois, L.W. Huang, and H.R. Bode. 1985. A subset of cells in the nerve net of *Hydra oligactis* defined by a monoclonal antibody: its arrangement and development. *Dev Biol*. 109:41-53.

Dupre, C., and R. Yuste. 2017. Non-overlapping Neural Networks in *Hydra vulgaris*. *Current Biology* 27:1085-1097.

Epp, L., and P. Tardent. 1978. The distribution of nerve cells in *Hydra attenuata* Pall. *Roux's Archives of Developmental Biology*. 185:185-193.

Galliot, B., M. Quiquand, L. Ghila, R. de Rosa, M. Miljkovic-Licina, and S. Chera. 2009. Origins of neurogenesis, a cnidarian view. *Dev Biol*. 332:2-24.

Giez, C., Pinkle, D., Giencke, Y., Wittlieb, J., Herbst, E., Spratte, T., Lachnit, T., Klimovich, A., Selhuber-Unkel, C., and T.C.G. Bosch. 2023a. Multiple neuronal populations control the eating behavior in *Hydra* and are responsive to microbial signals. *Curr Biol.* **33**:1-16.

Giez C., Noack C., Sakib, E., and T.C.G. Bosch. 2023b. The internal metabolic state controls behavior in *Hydra* through an interplay of enteric and central nervous system-like neuron populations. *bioRxiv* [Preprint]. doi.org/10.1101/2023.09.15.557876

Glauber, K.M., C.E. Dana, S.S. Park, D.A. Colby, Y. Noro, T. Fujisawa, A.R. Chamberlin, and R.E. Steele. 2013. A Small Molecule Screen Identifies a Novel Compound that Induces a Homeotic Transformation in *Hydra. Development*. 140:4788-4796.

Grimmelikhuijzen, C.J., I. Leviev, and K. Carstensen. 1996. Peptides in the nervous systems of cnidarians: structure, function, and biosynthesis. *Int Rev Cytol*. 167:37-89.

Grimmelikhuijzen, C.J.P. 1983. Coexistence of neuropeptides in *Hydra*. *Neuroscience*. 9:837-845.

Hadži, J. 1909. Über das Nervensystem von *Hydra*. *Arbeiten aus dem Zoologischen Institut der Universität Wien und der Zoologischen Station in Triest* 17:225 - 268.

Hager, G., and C.N. David. 1997. Pattern of differentiated nerve cells in *Hydra* is determined by precursor migration. *Development*. 124:569-576.

Hand, A.R., and S. Gobel. 1972. The structural organization of the septate and gap junctions of *Hydra*. *J Cell Biol*. 52:397-408.

Hansen, G.N., M. Williamson and C.J.P. Grimmelikhuijzen. 2000. Two-color double-labeling in situ hybridization of whole mount *Hydra* using RNA probes for five different *Hydra* neuropeptide preprohormones: evidence for co-localization. *Cell Tissue Research* 301: 245-253

Hobmayer, E., T.W. Holstein, and C.N. David. 1990a. Tentacle Morphogenesis in *Hydra*. 1. The Role of Head Activator. *Development*. 109:887-895.

Hobmayer, E., T.W. Holstein, and C.N. David. 1990b. Tentacle Morphogenesis in *Hydra*. 2. Formation of a Complex between a Sensory Nerve-Cell and a Battery Cell. *Development*. 109:897-904.

Holstein, T.W. 2023. Neuronal control of an archaic mouth. *Current Biology* **33**:R###-###.

Hufnagel, L., and G. Kass-Simon. 1976. The Ultrastructural Basis for the Electrical Coordination Between Epithelia of *Hydra*. *In* Coelenterate Ecology and Behavior. G.O. Mackie, editor. Springer US, Boston, MA. 695-704.

Juliano, C. E., Lin, H., and R.E. Steele. 2014. Generation of transgenic *Hydra* by embryo microinjection. *J Vis Exp*(91), 51888.

Kinnamon, J.C., and J.A. Westfall. 1981. A three dimensional serial reconstruction of neuronal distributions in the hypostome of a *Hydra*. *J Morphol*. 168:321-329.

Kinnamon, J.C., and J.A. Westfall. 1982. Types of neurons and synaptic connections at hypostome-tentacle junctions in *Hydra*. *J Morphol*. 173:119-128.

Koizumi, O. 2007. Nerve ring of the hypostome in *Hydra*: is it an origin of the central nervous system of bilaterian animals? *Brain, behavior and evolution*. 69:151-159.

Koizumi, O., Itazawa, M., Mizumoto, H., Minobe, S., Javois, L. C., Grimmelikhuijzen, C. J., and H.R. Bode. 1992. Nerve ring of the hypostome in *Hydra*. I. Its structure, development, and maintenance. *J Comp Neurol, 326*, 7-21.

Koizumi, O., Sato, N., and C. Goto. 2004. Chemical anatomy of *Hydra* nervous system using antibodies against *Hydra* neuropeptides: a review. *Hydrobiologia, 530*, 41-47.

Mackie, G. 1990. The Elementary Nervous System Revisited. *American Zoologist*. 30:907-920.

Marcum, B.A., and R.D. Campbell. 1978. Development of *Hydra* lacking nerve and interstitial cells. *J Cell Sci*. 29:17-33.

Matsuno, T., and T. Kageyama. 1984. The nervous system in the hypostome of *PelmatoHydra robusta*: The presence of a circumhypostomal nerve ring in the epidermis. *J Morphol*. 182:153-168.

Noro, Y., S. Yum, C. Nishimiya-Fujisawa, C. Busse, H. Shimizu, K. Mineta, X. Zhang, T.W. Holstein, C.N. David, T. Gojobori, and T. Fujisawa. 2019. Regionalized nervous system in *Hydra* and the mechanism of its development. *Gene Expr Patterns*. 31:42-59.

Primack, A.S., Cazet, J.F., Little, H-M., Mühlbauer, S., Cox, B.D., David, C.N., Farrell, J.A., and C.E. Juliano (2023). Differentiation trajectories of the *Hydra* nervous system reveal transcriptional regulators of neuronal fate. *bioRxiv* [Preprint]. doi: 10.1101/2023.03.15.531610.

Riedl, J., A.H. Crevenna, K. Kessenbrock, J.H. Yu, D. Neukirchen, M. Bista, F. Bradke, D. Jenne, T.A. Holak, Z. Werb, M. Sixt, and R. Wedlich-Soldner. 2008. Lifeact: a versatile marker to visualize F-actin. *Nat Methods*. 5:605-607.

Schneider, K.C. 1890. Histologie von *Hydra fusca* mit besonderer Berücksichtigung des Nervensystems der Hydropolypen. *Archiv Für Mikroskopische Anatomie*. 35:321-379.

Shimizu, H., O. Koizumi, and T. Fujisawa. 2004. Three digestive movements in *Hydra* regulated by the diffuse nerve net in the body column. *J Comp Physiol A Neuroethol Sens Neural Behav Physiol*. 190:623-630.

Shimizu, H., Y. Takaku, X. Zhang, and T. Fujisawa. 2007. The aboral pore of *Hydra*: evidence that the digestive tract of *Hydra* is a tube not a sac. *Dev Genes Evol*. 217:563-568.

Siebert, S., J.A. Farrell, J.F. Cazet, Y. Abeykoon, A.S. Primack, C.E. Schnitzler, and C.E. Juliano. 2019. Stem cell differentiation trajectories in *Hydra* resolved at single-cell resolution. *Science*. 365, eaav9314.

Szymanski, J.R., and R. Yuste. 2019. Mapping the Whole-Body Muscle Activity of *Hydra vulgaris*. *Curr Biol*. 29:1807-1817 e1803.

Takahashi, T., Y. Kobayakawa, Y. Muneoka, Y. Fujisawa, S. Mohri, M. Hatta, H. Shimizu, T. Fujisawa, T. Sugiyama, M. Takahara, K. Yanagi, and O. Koizumi. 2003. Identification of a new member of the GLWamide peptide family: physiological activity and cellular localization in cnidarian polyps. *Comp Biochem Physiol B Biochem Mol Biol*. 135:309-324.

Takaku, Y., J.S. Hwang, A. Wolf, A. Bottger, H. Shimizu, C.N. David, and T. Gojobori. 2014. Innexin gap junctions in nerve cells coordinate spontaneous contractile behavior in *Hydra* polyps. *Sci Rep*. 4:3573.

Technau, U., and T.W. Holstein. 1996. Phenotypic maturation of neurons and continuous precursor migration in the formation of the peduncle nerve net in *Hydra*. *Dev Biol*. 177:599-615.

Wanek, N., B. Marcum, H.-T. Lee, M. Chow, and R. Campbell. 1980. Effect of hydrostatic pressure on morphogenesis in nerve-free *Hydra*. *Journal of Experimental Zoology*. 211:275-280.

Wang, H., J. Swore, S. Sharma, J. Szymanski, R. Yuste, T. Daniel, M. Regnier, M. Bosma, and A. Fairhall. 2023. A complete biomechanical model of Hydra contractile behaviors, from neural drive to muscle to movement. Proceedings of the National Academy of Sciences 120, e2210439120.10.1073/PNAS.2210439120.

Watanabe, H., T. Fujisawa, and T.W. Holstein. 2009. Cnidarians and the evolutionary origin of the nervous system. *Dev Growth Differ*. 51:167-183.

Westfall, J.A. 1973. Ultrastructural evidence for a granule-containing sensory-motor-interneuron in *Hydra littoralis*. *J Ultrastruct Res*. 42:268-282.

Westfall, J.A. and L. Epp. 1985. Scanning electron microscopy of neurons isolated from the pedal disk and the body column of *Hydra*. *Tissue & Cell* 17:161-170.

Westfall, J.A., D.R. Argast, and J.C. Kinnamon. 1983. Numbers, distribution, and types of neurons in the pedal disk of *Hydra* based on a serial reconstruction from transmission electron micrographs. *J Morphol*. 178:95-103.

Westfall, J.A., J.C. Kinnamon, and D.E. Sims. 1980. Neuro-epitheliomuscular cell and neuro-neuronal gap junctions in *Hydra*. *J Neurocytol*. 9:725-732.

Westfall, J.A., S. Yamataka, and P.D. Enos. 1971. Ultrastructural evidence of polarized synapses in the nerve net of *Hydra*. *J Cell Biol*. 51:318-323.

Wittlieb, J., K. Khalturin, J.U. Lohmann, F. Anton-Erxleben, and T.C. Bosch. 2006. Transgenic *Hydra* allow in vivo tracking of individual stem cells during morphogenesis. *Proc Natl Acad Sci U S A*. 103:6208-6211.

Yamamoto, W., and R. Yuste. 2020. Whole-Body Imaging of Neural and Muscle Activity during Behavior in *Hydra vulgaris*: Effect of Osmolarity on Contraction Bursts. *eNeuro*. 7.

Yaross, M.S., and H.R. Bode. 1978a. Regulation of interstitial cell differentiation in *Hydra attenuata*. III. Effects of I-cell and nerve cell densities. *J Cell Sci*. 34:1-26.

Yaross, M.S., and H.R. Bode. 1978b. Regulation of interstitial cell differentiation in *Hydra attenuata*. IV. Nerve cell commitment in head regeneration is position-dependent. *J Cell Sci*. 34:27-38.

Yaross, M.S., J. Westerfield, L.C. Javois, and H.R. Bode. 1986. Nerve cells in *Hydra*: monoclonal antibodies identify two lineages with distinct mechanisms for their incorporation into head tissue. *Dev Biol*. 114:225-237.

Figure 1

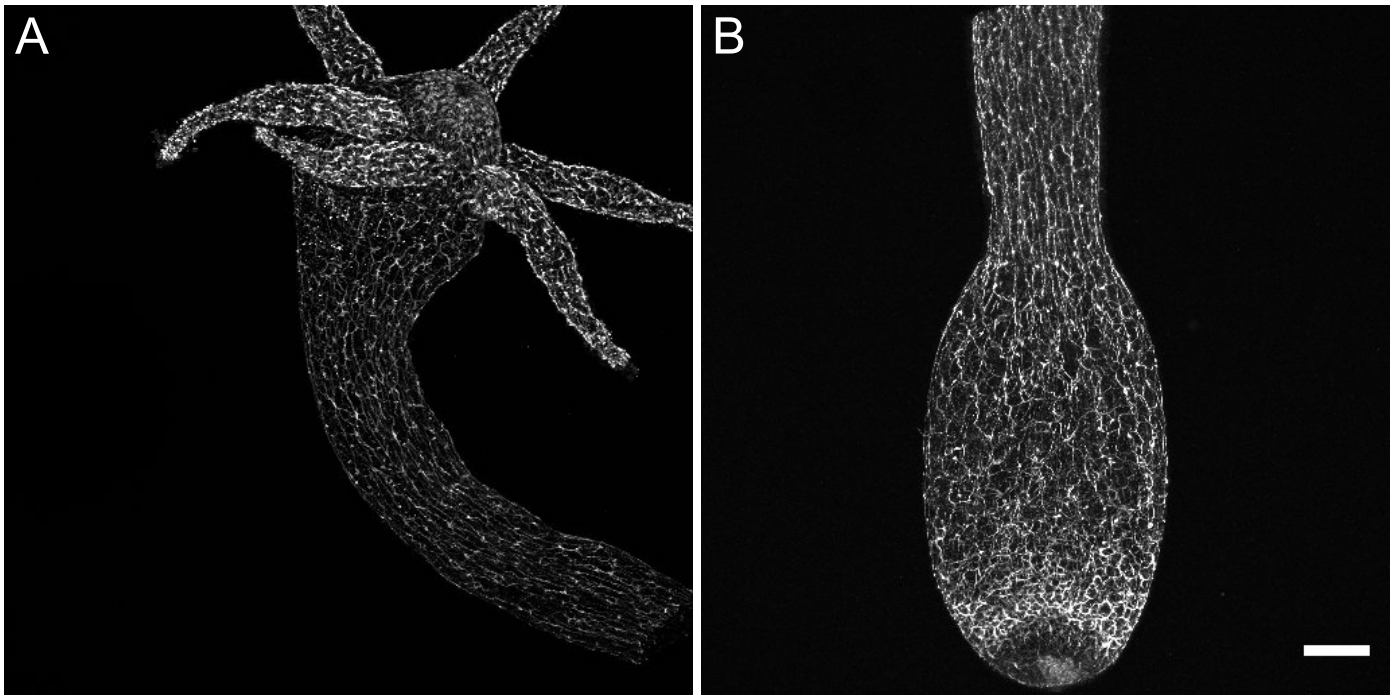

Figure 2

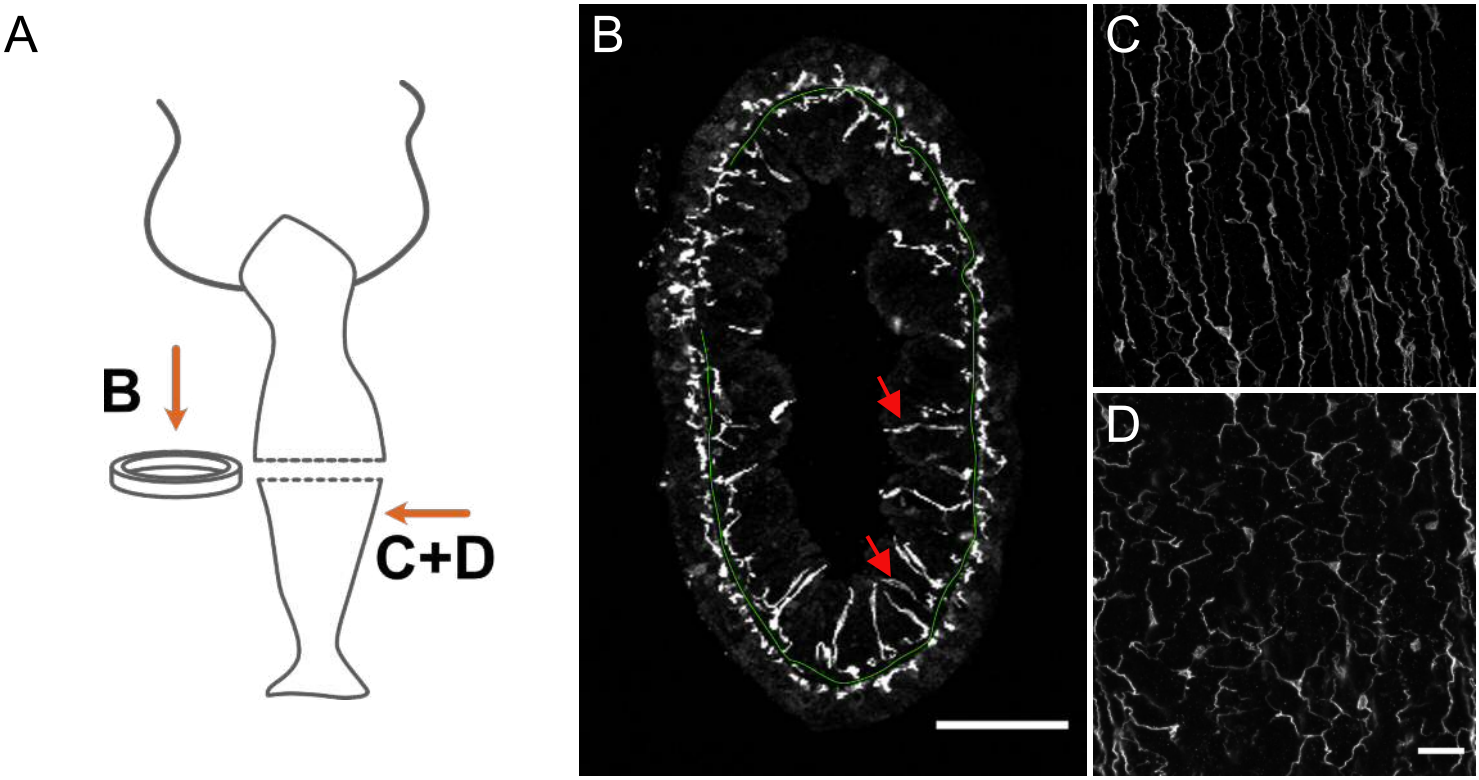

Figure 3

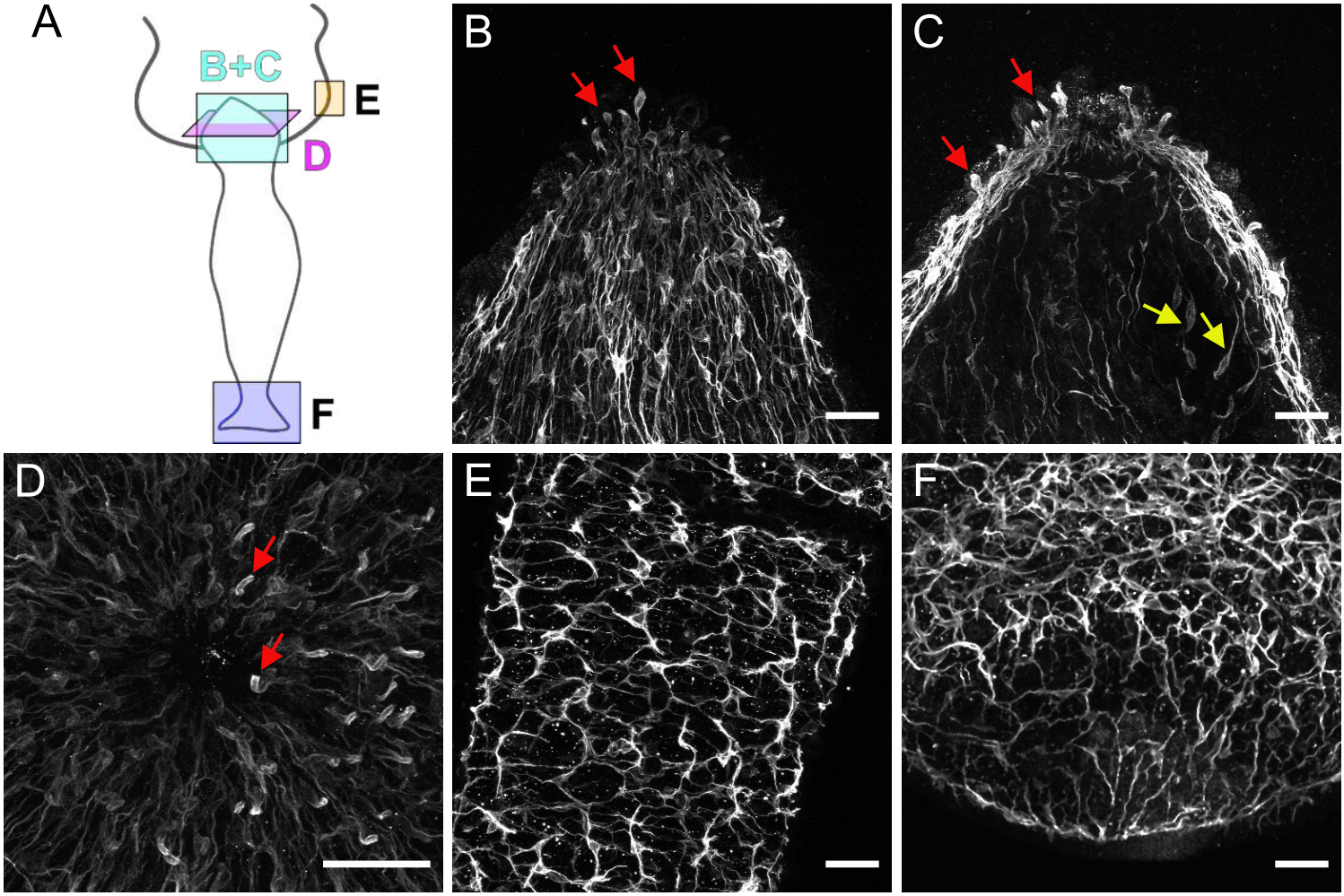

Figure 4

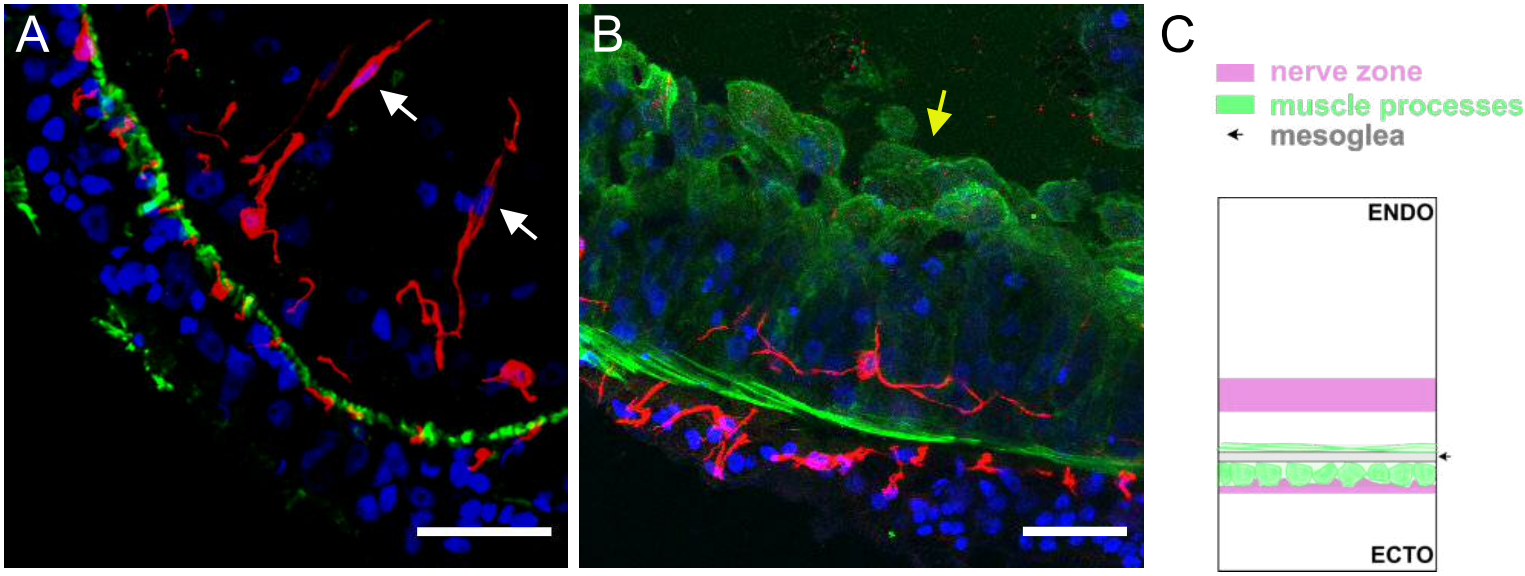

Figure 5

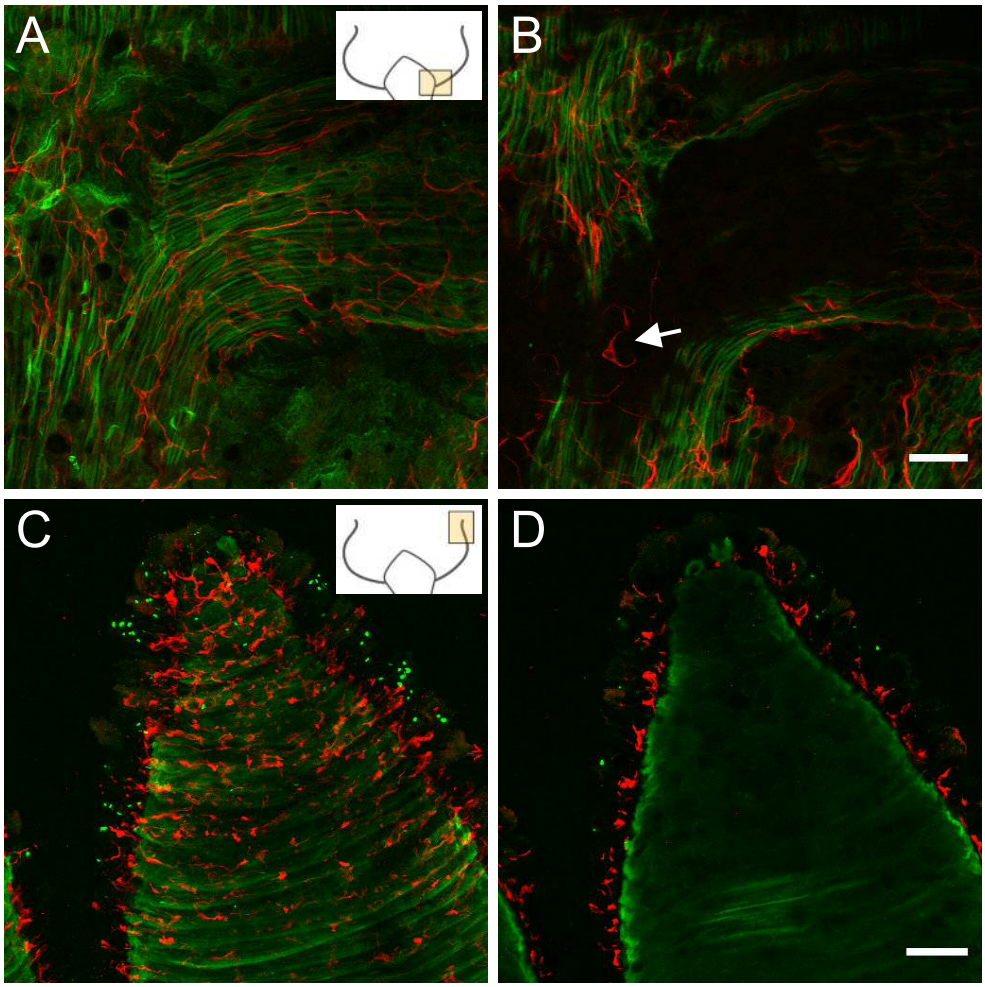

Figure 6

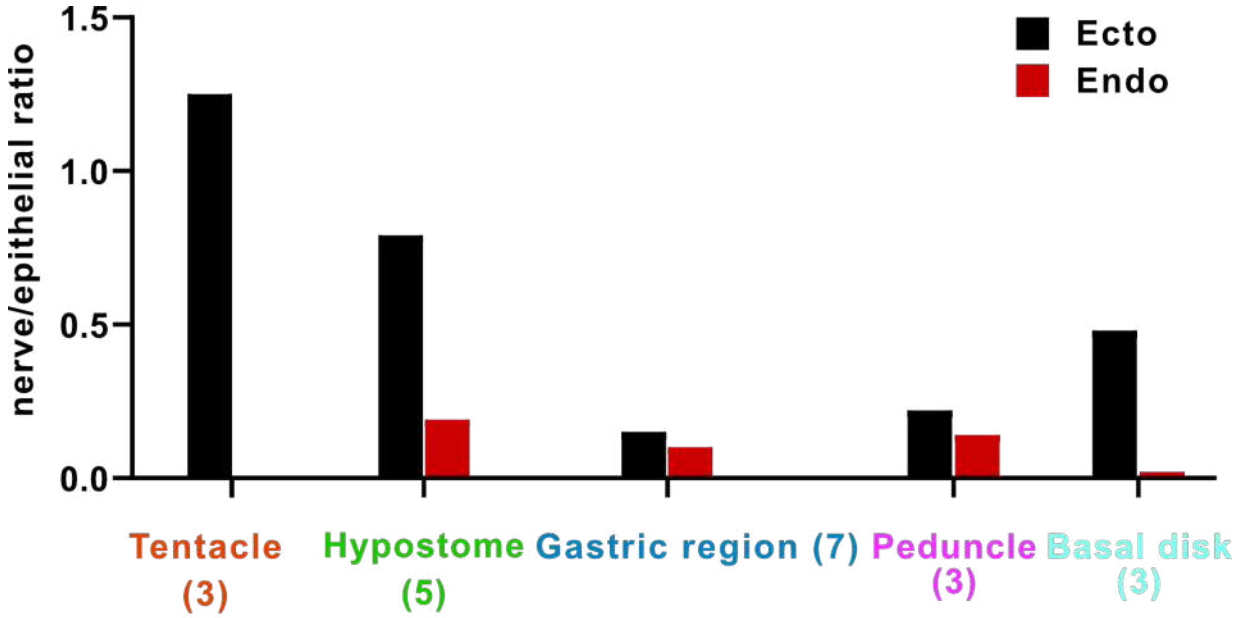

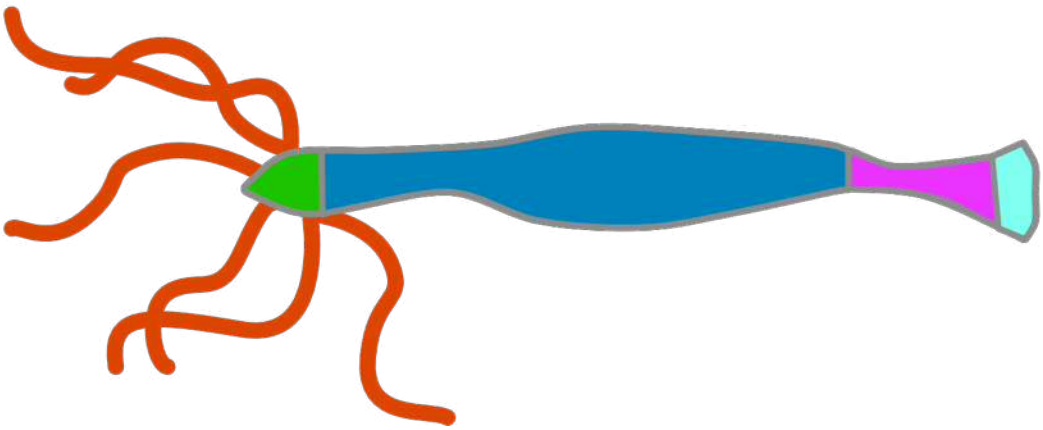

Figure 7

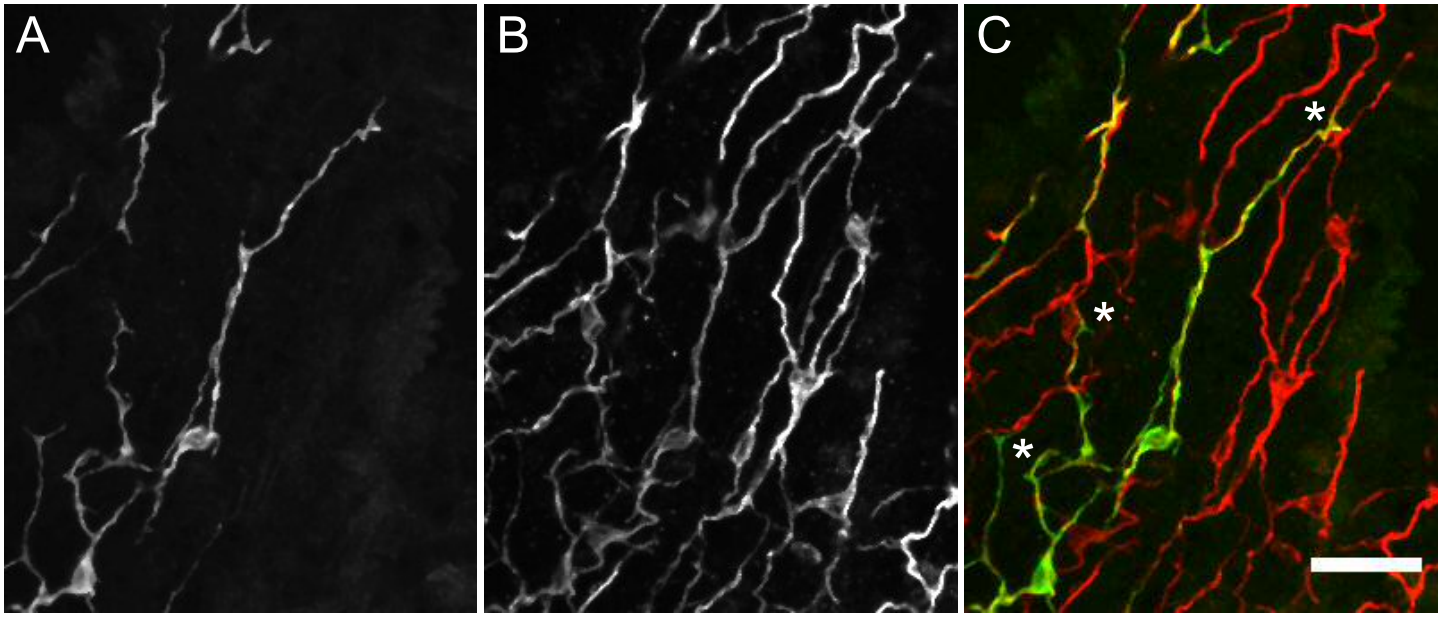

Figure 8

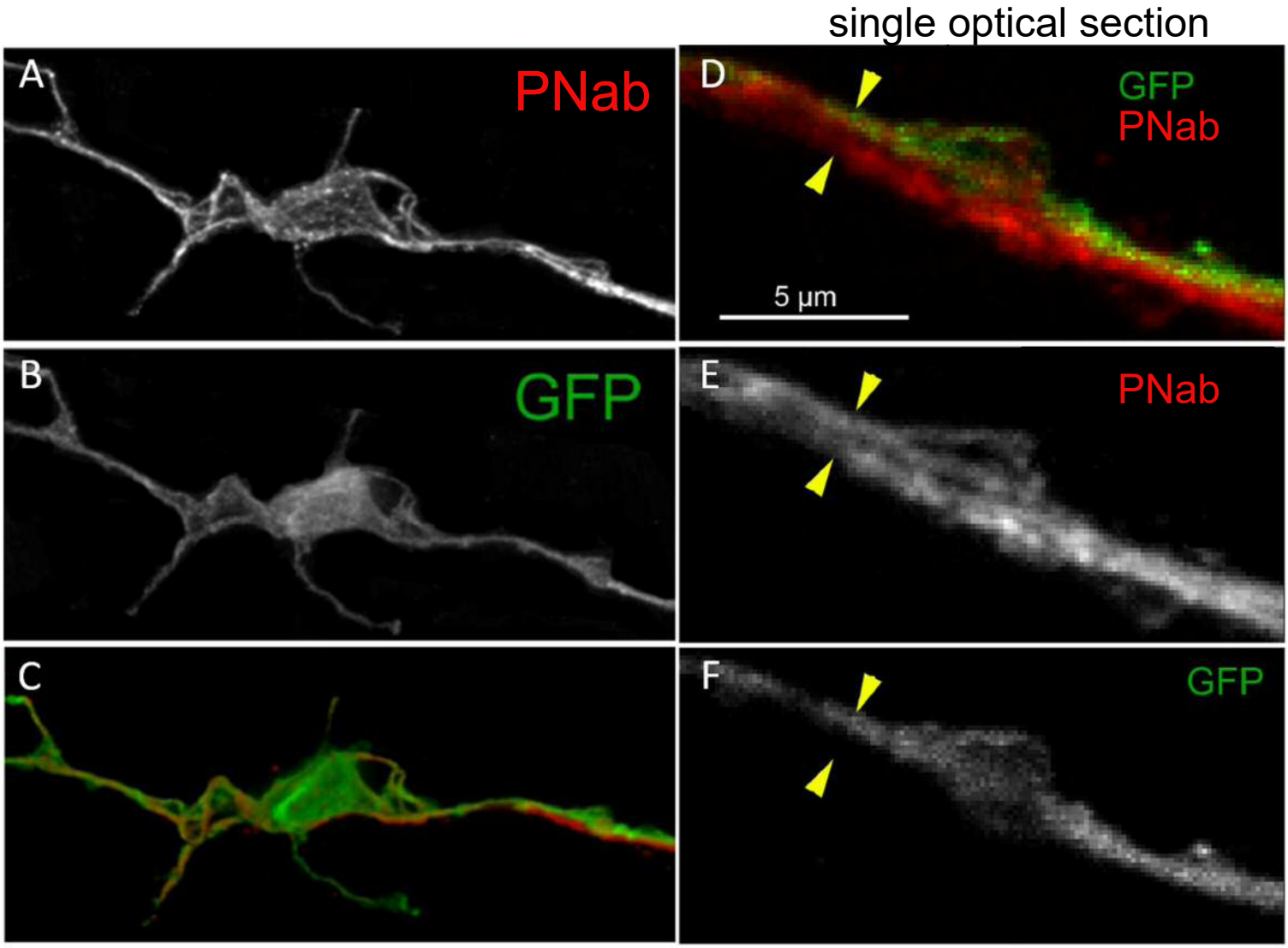

Figure 9

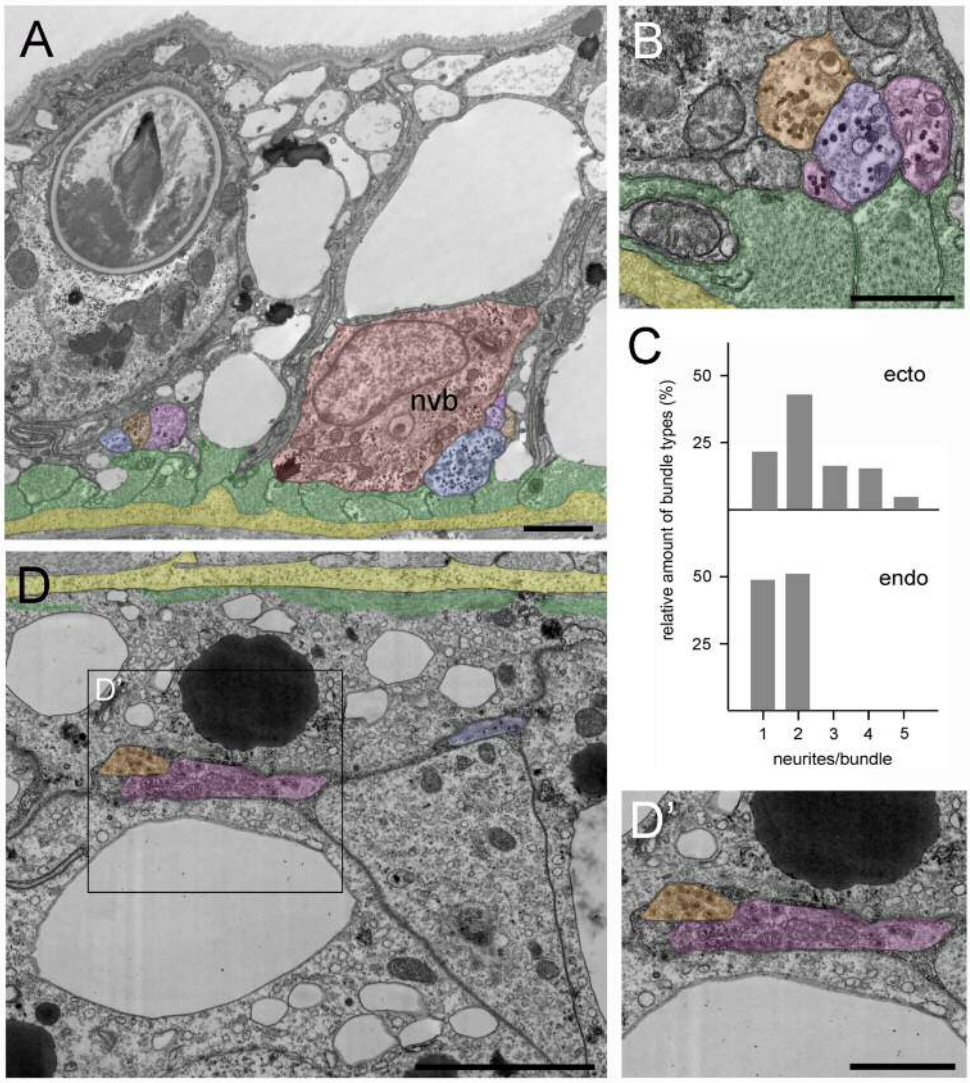

Figure 10

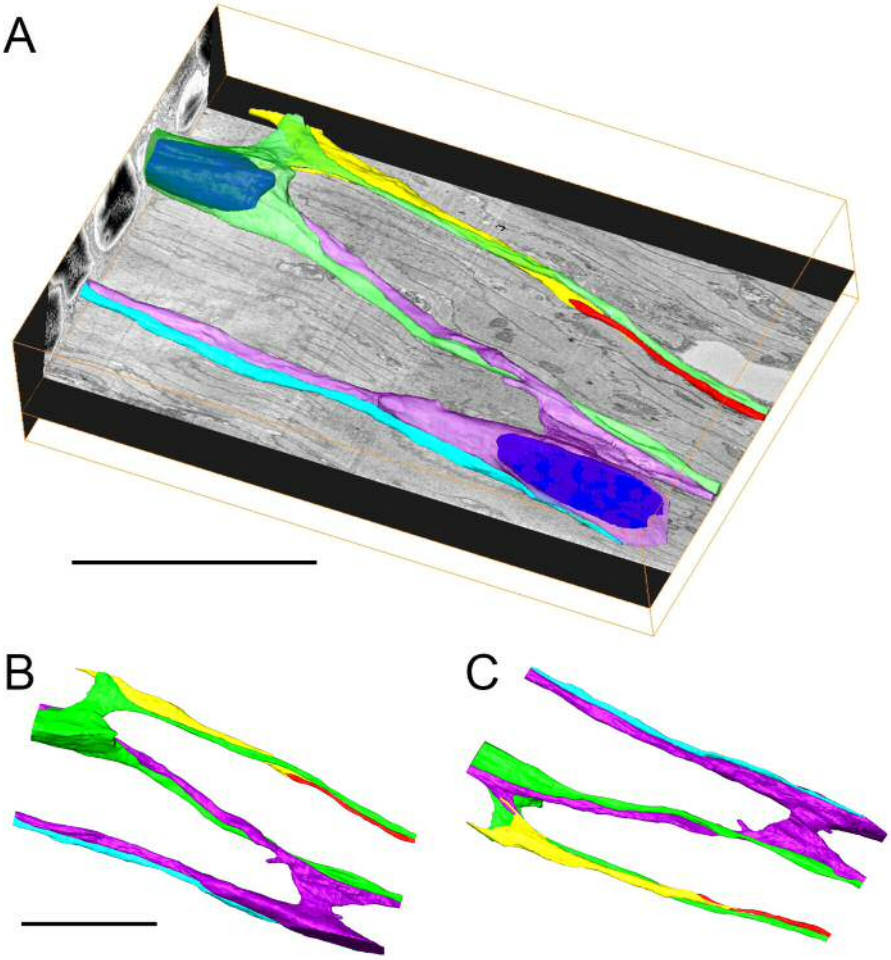

Figure 11

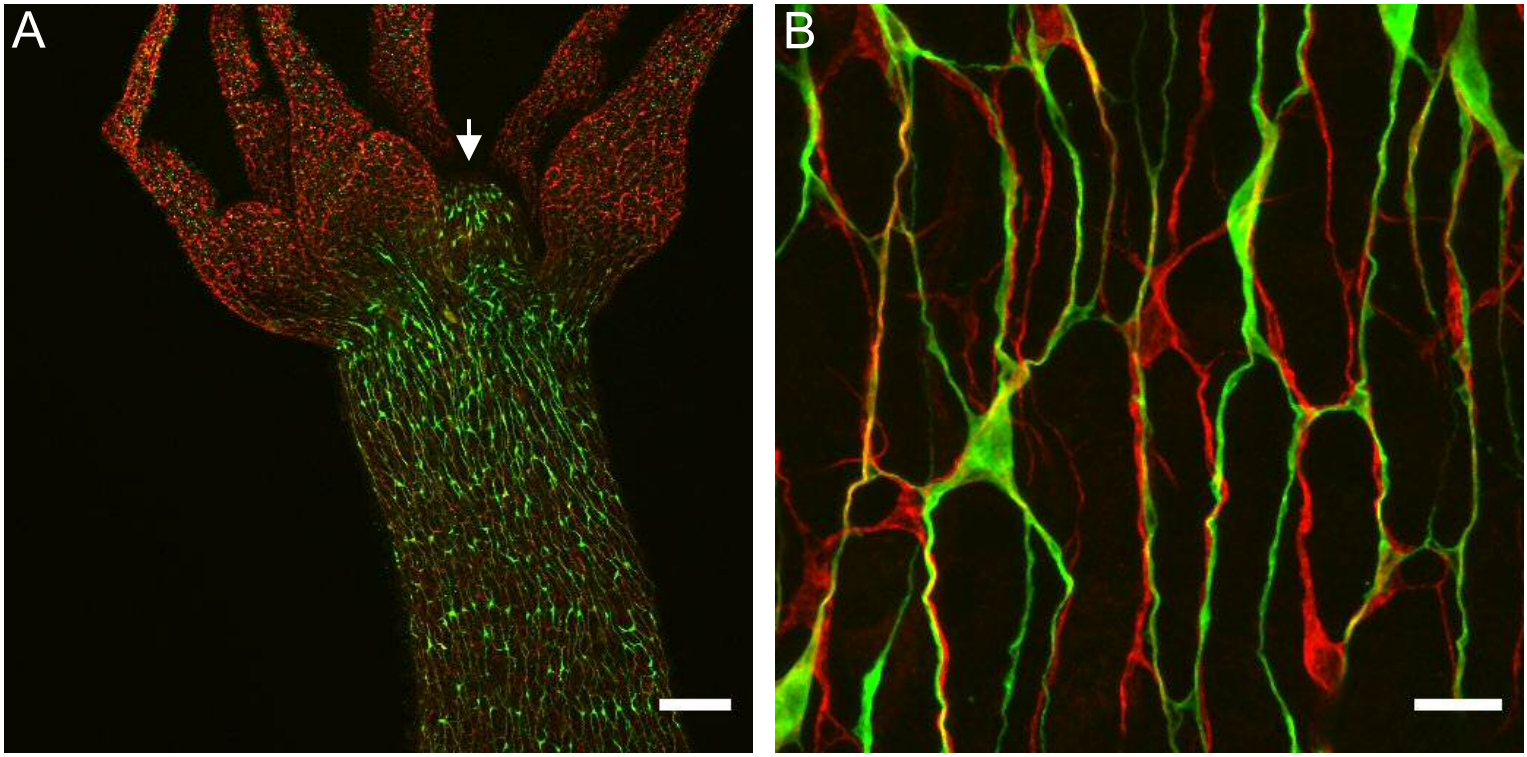

Figure 12

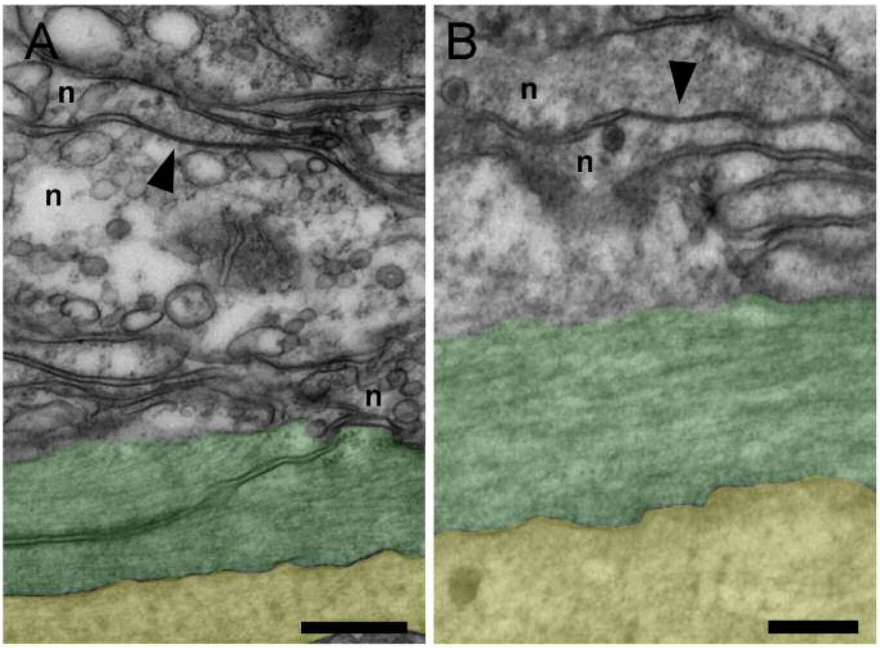
A
n
n
n
B
n
n

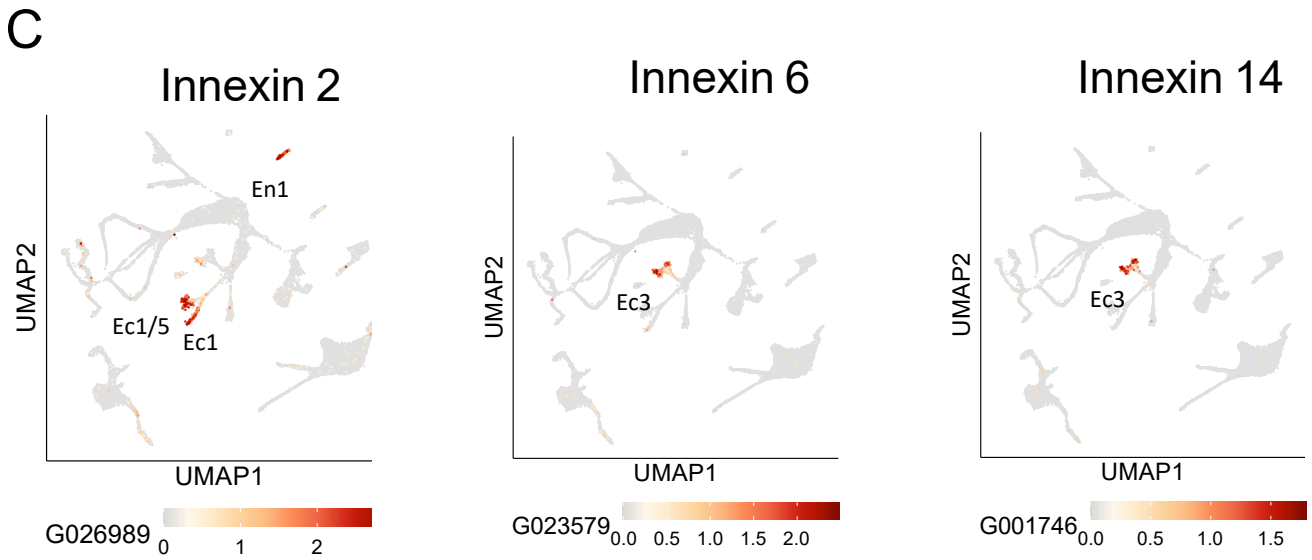
C
Innexin 2
Innexin 6
Innexin 14
UMAP2
UMAP1
En1
Ec1/5
Ec1
G026989
0
1
2
UMAP2
UMAP1
Ec3
G023579
0.0
0.5
1.0
1.5
2.0
UMAP2
UMAP1
Ec3
G001746
0.0
0.5
1.0
1.5

Figure 13

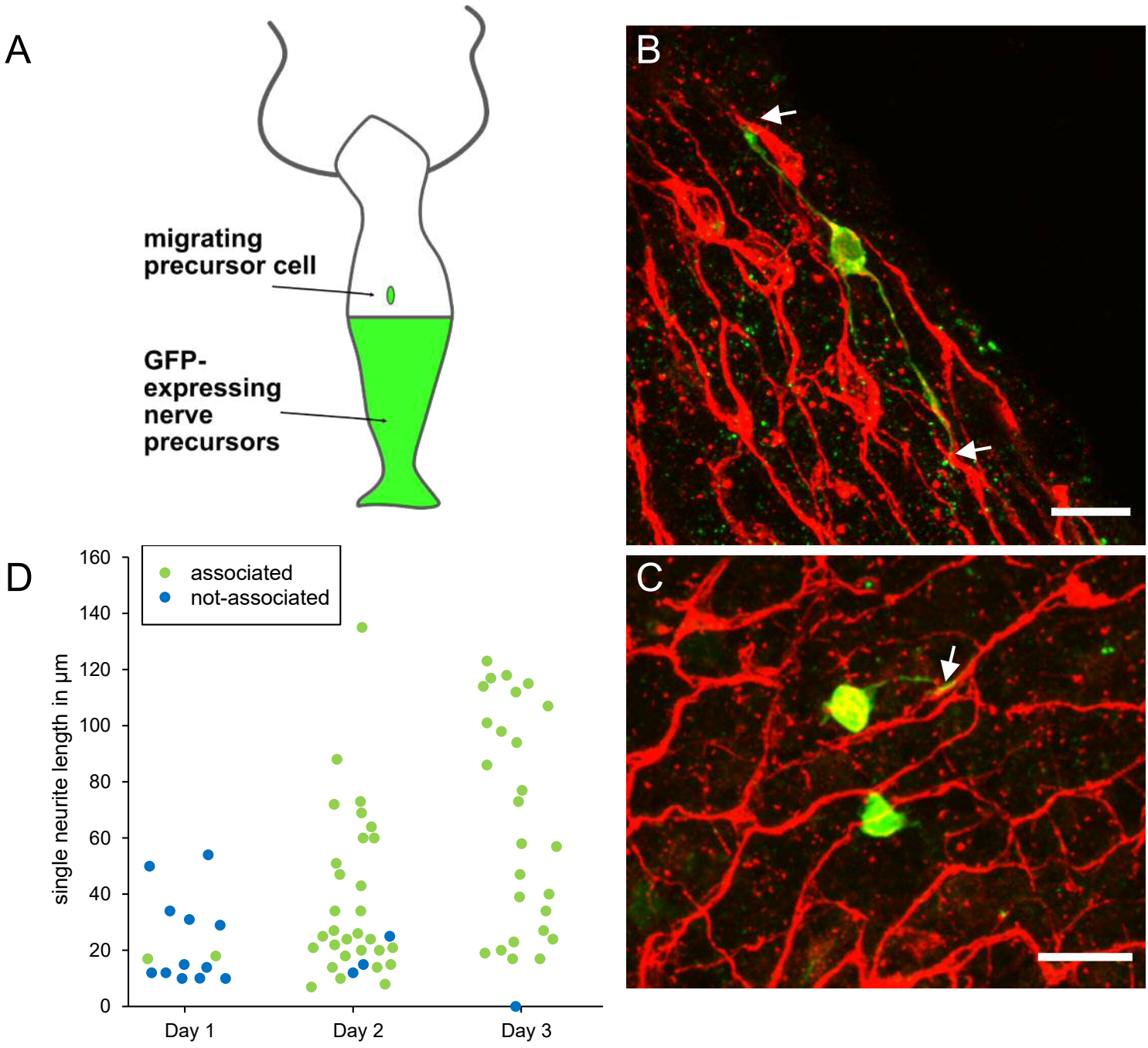
A
migrating precursor cell
GFP-expressing nerve precursors
B
C
D
associated
not-associated
single neurite length in µm
160
140
120
100
80
60
40
20
0
Day 1
Day 2
Day 3

Figure 14

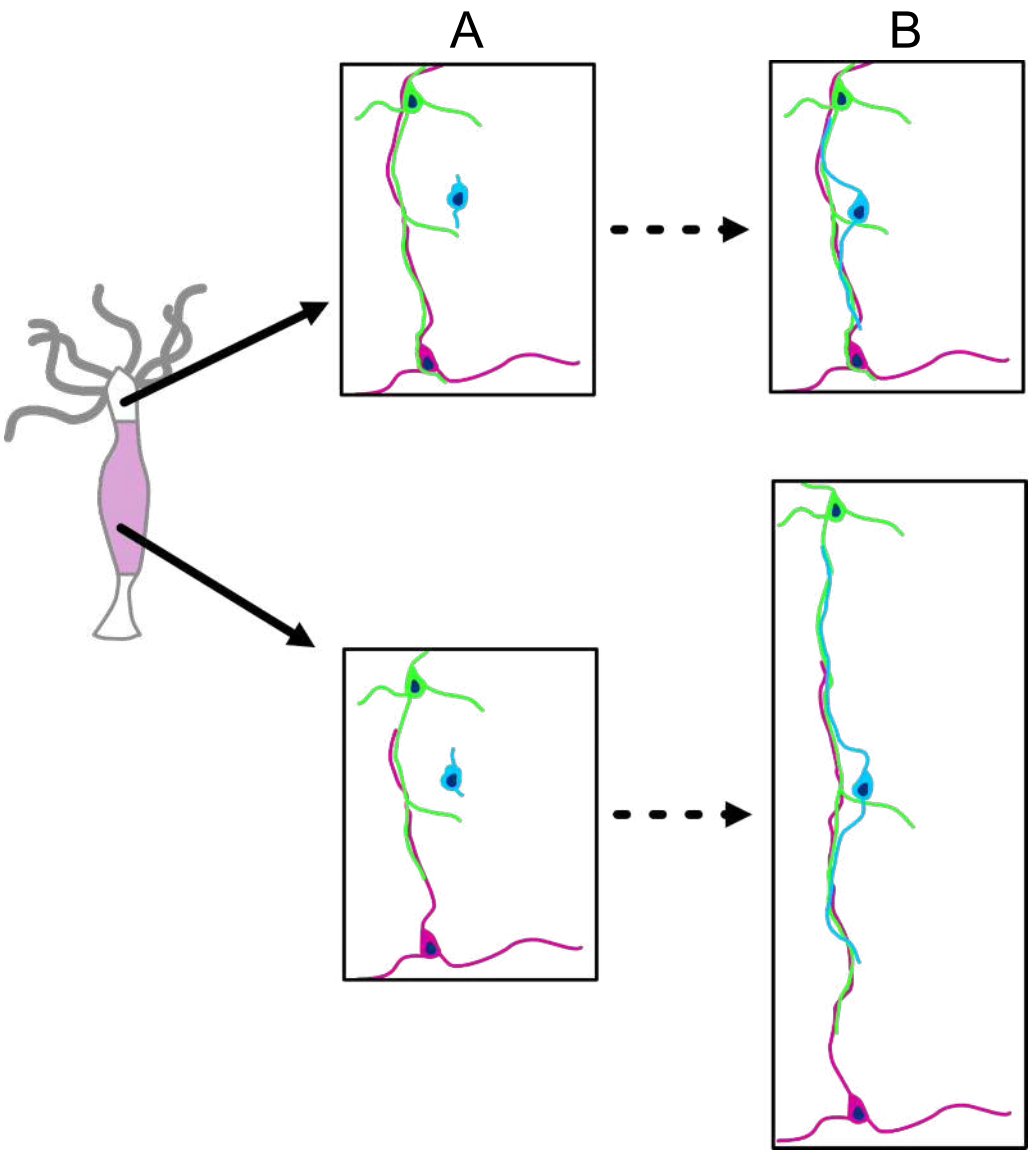

Suppl Figure 1

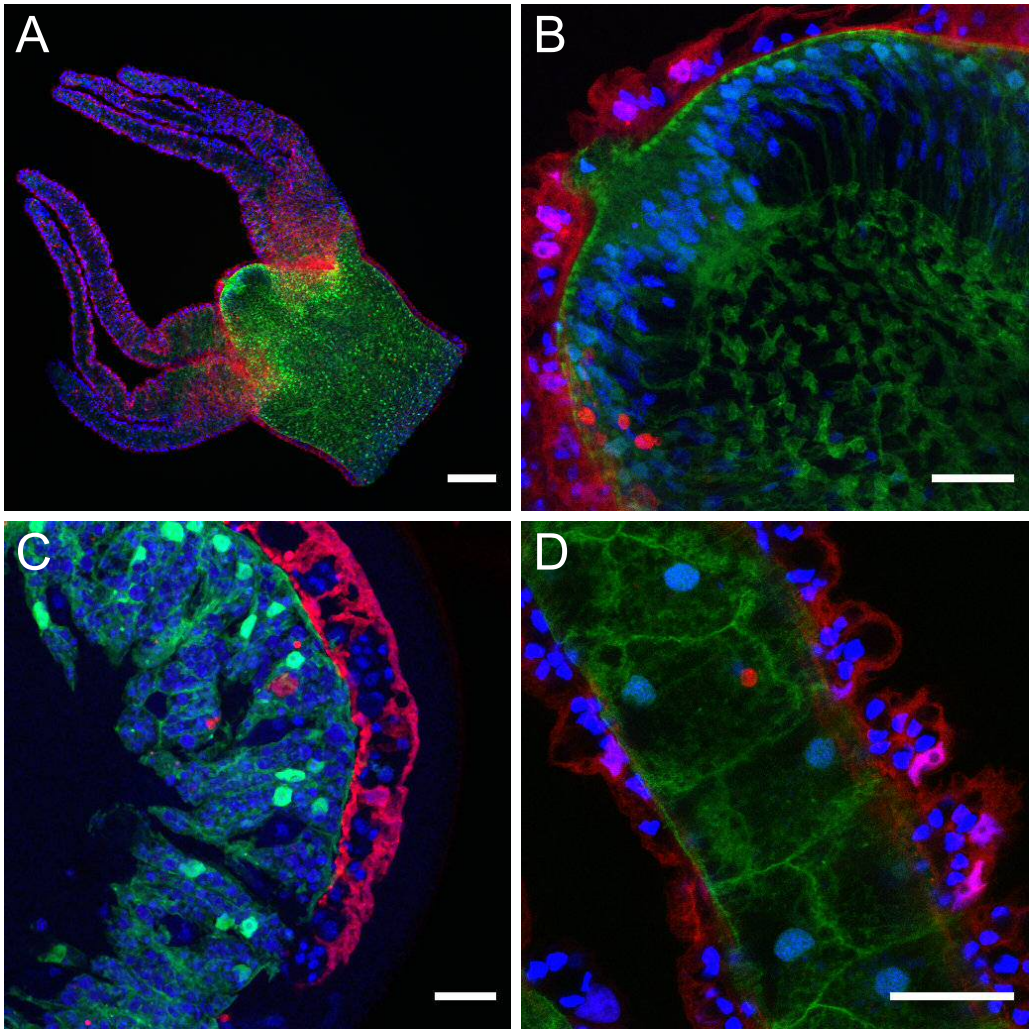

Suppl Figure 2

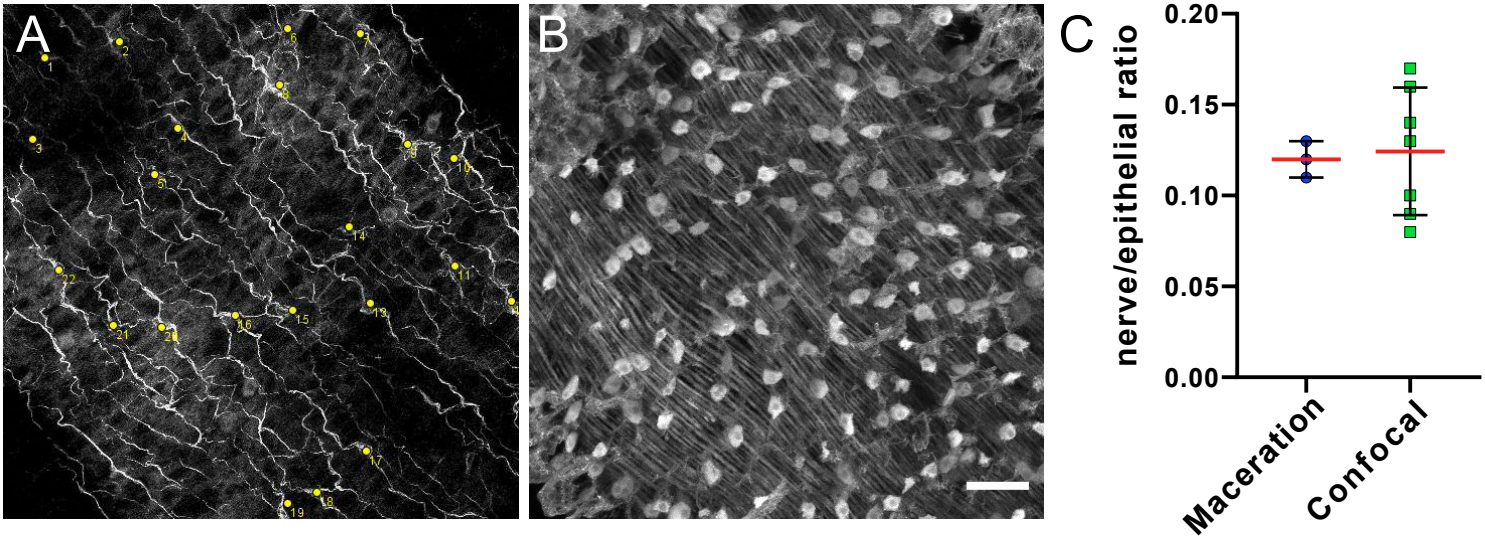

Suppl Figure 3

p120/δ-Catenin binding domain

```
H.vul.105      KKKPIPIYVDQTCRENVMLYADEGAGEDDFHNYDLE-LLQHAGGKNLSVVEDMNSFEMSEINKNGYSFIGGSQNDFSNERNSFIHDSNTRIYNSSNGEAYNAT  102
H.oli.Ibk12    KKKPIPIYVDQSCRENIMLYADEGAGEDDFHNYDLEKLLQHAGGKNLTIIED---FEMNEINKNGYSFIGGSQKEFLNDRNSFIYDSNTRI-----SNIYNA-   94
H.vir.A99      KKKPIPIYVDQSCRENVMLYADEGAGEDDYHQYDLEKLLQHAGGRNLTIIDDADGFEMNEMSLMKNDFI---------------HDQVNEINRVNEKNAYNSI   88
```

antibody peptide antigen

```
H.vul.105      TARSVSNAFNSS----NNEAYNATTARSVSNAYNN-SSQSAGEMYRATTARST------VTRNQQDQQENRFSNQNESESLLRSDYNA--NTETANFTSRSQR  192
H.oli.Ibk12    ---------N-S----SNEAYNASTARSVSNAYNASTSQSAGDMFKSTTARST-------------GEKFEFNSRNESESLLQSDYNTKSNIETANFTSRSQR  170
H.vir.A99      SARSLGDAYNASSARSMGETYNATSARFTGEMYNTTSARSAGEMYNATSTFSAGEMHNASSVRSTKENRYEYKSQNESESLMRSEASASRT--------QRQF  183
```

β-Catenin binding domain

```
H.vul.105      QVSQSSRFDA-SQAEEINLALFIDEQLLAADNSKNSHPRDTLLHYGYEGEGSDMSDLSELGESESETDDEDDFSFLADWGPKFEFLDRLYNPRTDDSEEDV    292
H.oli.Ibk12    QVSQSSRFDA-TQAEEINLALFIDEQLLAADNSKISHPRDTLLHYGYEGEGSDMSDLSELGESESESEDEDDFSFLADWGPKFEFLDRLYNPRTDDSEEDV    270
H.vir.A99      QHNGSSRFDAKAQAEEINLSEFINEKLFAADNANNSHPRDTLLHYGYEGEGSDMSDLSELGDSDSESEDEDDFSFLADWGPKFELLDRLYNPRTDDSEEDV    284
```

```
H. vulgaris (strain magnipapillata 105): Chapman et al., 2010
H. oligactis (strain Innsbruck female 12): Cazet et al., 2023
H. viridissima (strain A99): Hamada et al., 2020
```

Suppl Figure 4

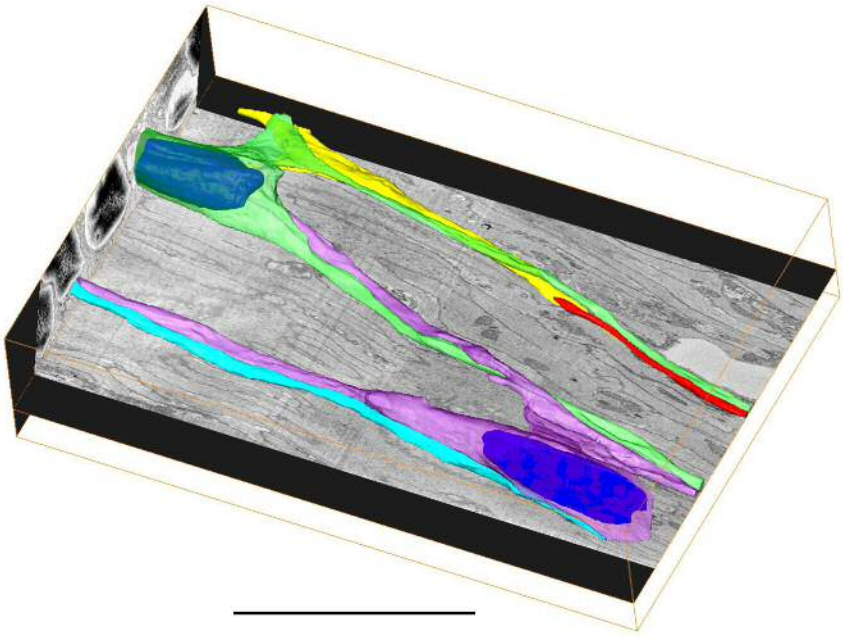

Fig. 10 Supplement 3D interactive

3D reconstruction of 2000 serial sections obtained by serial block face scanning SEMin the ectoderm of the body column. Two nerve cell bodies and their neurites are colored green and purple (nuclei are highlighted in blue). Three addinional neurites from nerve cells outside the imaged block are colored yellow, red and blue. The imaged block is 56 µm long. Scale bar: 20 µm.

The interactive 3D model can be accessed by clicking into Figure 10 (Adobe Reader Version 7 or higher required). Rotate model by dragging with left mouse button pressed, shift model: same action + ctrl, zoom: use mouse wheel (or change default action for left mouse button). Select or deselect (or change transparency of) components in the model tree, **switch between prefab views** or change surface visualization (e.g., lightning, render mode, crop, etc.).